Available online at www.sciencedirect.com
ScienceDirect
Earth-Science Reviews 81 (2007) 93–134
EARTH-SCIENCE REVIEWS
www.elsevier.com/locate/earscirev

North American drought: Reconstructions, causes, and consequences

Edward R. Cook [a,*], Richard Seager [a], Mark A. Cane [a], David W. Stahle [b]

[a] *Lamont-Doherty Earth Observatory, Palisades, NY 10964 USA*
[b] *Department of Geosciences, University of Arkansas, Fayetteville, AR 72701 USA*

Received 29 December 2005; accepted 18 December 2006
Available online 3 January 2007

Abstract

Severe drought is the greatest recurring natural disaster to strike North America. A remarkable network of centuries-long annual tree-ring chronologies has now allowed for the reconstruction of past drought over North America covering the past 1000 or more years in most regions. These reconstructions reveal the occurrence of past "megadroughts" of unprecedented severity and duration, ones that have never been experienced by modern societies in North America. There is strong archaeological evidence for the destabilizing influence of these past droughts on advanced agricultural societies, examples that should resonate today given the increasing vulnerability of modern water-based systems to relatively short-term droughts. Understanding how these megadroughts develop and persist is a timely scientific problem. Very recently, climate models have succeeded in simulating all of the major droughts over North America from the Civil War to the severe 1998–2004 drought in the western U.S. These numerical experiments indicate the dominating importance of tropical Pacific Ocean sea surface temperatures (SSTs) in determining how much precipitation falls over large parts of North America. Of central importance to drought formation is the development of cool "La Niña-like" SSTs in the eastern tropical Pacific region. This development appears to be partially linked to changes in radiative forcing over that region, which affects the Bjerknes feedback mechanism of the ENSO cycle there. Paradoxically, warmer conditions over the tropical Pacific region lead to the development of cool La Niña-like SSTs there, which is drought inducing over North America. Whether or not this process will lead to a greater prevalence of drought in the future as the world warms due to accumulating greenhouse gases is unclear at this time.
© 2007 Elsevier B.V. All rights reserved.

Keywords: North American drought; Palmer drought index; tree rings; drought reconstructions; drought causes and consequences; ENSO variability

1. Introduction

The western United States (the 'West') has been in the grip of a severe drought since late 1999, which only recently (mid-2005) appears to be ending (U.S. Drought Monitor; http://www.drought.unl.edu/dm/monitor.html; Svoboda et al., 2002). Whether or not this change towards wetter conditions truly represents the end of this severe multi-year drought remains to be seen. However, at its peak in July 2002, more than 50% of the contiguous U.S. was under moderate to severe drought conditions, with record or near-record precipitation deficits throughout the West (Lawrimore and Stephens, 2003). Large portions of the Canadian Prairie provinces also suffered from severe drought (Agricultural and Agri-Food Canada, 2002), as well as extensive areas of Mexico, particularly in the northern and western parts of the country (Lawrimore et al., 2002; consult the March 2003 drought map and associated report located at the North American Drought Monitor website address provided with the reference).

* Corresponding author. Tel.: +1 845 365 8618; fax: +1 845 365 8152.
E-mail address: drdendro@ldeo.columbia.edu (E.R. Cook).

0012-8252/$ - see front matter © 2007 Elsevier B.V. All rights reserved.
doi:10.1016/j.earscirev.2006.12.002

The impacts of this drought on the West have been considerable. Four consecutive years of drought resulted in water supply deficits in reservoir storage, with 10 of 11 western states having below average storage by May 2004, and below 50% capacity in Arizona, New Mexico, Nevada, Utah, and Wyoming (USDA, 2004). By September 22, 2004, the elevation of Lake Powell was down 129 ft from full pool level, only 38% of *live* capacity (Upper Colorado Region Water Operations Data; http://www.usbr.gov/uc/crsp/GetSiteInfo). Most of this water loss from Lake Powell occurred in only three years beginning with the epic 2002 drought year, down from a lake level that was near its historic maximum in early 2000. Exacerbated by drought conditions, the 2002 fire season was the second worst in the last 50 yr, with wildfire burning over 370,000 ha, including the largest fires in the past century in Oregon, Arizona, and Colorado (NASA, 2004). Persistent drought in the American Southwest in combination with associated insect outbreaks also resulted in over three million acres of pinyon and ponderosa pine mortality in Arizona and New Mexico (Betancourt, 2003), with die-off spreading into southwestern Colorado as well. This drought highlights both the extreme vulnerability of the semi-arid West to shortfalls in precipitation and the need to better understand long-term drought variability and its causes in North America.

The impact of drought on the environment is obvious. Perhaps less obvious is its surprisingly high economic cost. Over the years 1980 to 2003, for the United States as a whole, droughts (and associated heat waves) accounted for 10 of the 58 weather-related disasters that are estimated to have cost more than one billion dollars (normalized to 2002 dollars; Ross and Lott, 2003). Those drought disasters (17.2% of the total) accounted for $144 billion (41.2%) of the estimated $349 billion total cost of all weather-related disasters (Ross and Lott, 2003). This is considerably more, at least until Hurricane Katrina struck the Gulf Coast, than the cost of hurricanes and tropical storms, the most frequent source of billion-dollar disasters: (16 events and 102 billion dollars over the same time period). So, in economic terms alone, droughts are the most costly natural disasters to strike the United States.

Drought maps of three notable billion-dollar drought years are shown in Fig. 1: 1980, 1988, and 2002. The estimated cost of the 2002 drought year was at $10 billion far less than the estimated cost of droughts in 1980 ($48.8 billion) and 1988 ($61.6 billion). So even though the 2002 drought year was extreme, and in some areas of the West unprecedented, its overall economic impact was comparatively low. The reason for this is probably related to where the 2002 drought happened, i.e., mostly in the inter-montane West where population density and agricultural production are relatively low. In contrast, the 1980 and 1988 droughts occurred especially over the northern and eastern Great Plains (see also Fye et al., 2004), regions of more intensive agriculture and greater population density. The number of human deaths from those droughts and associated heat waves was also high in 1980 (~10,000 deaths) and 1988 (~7500 deaths), but zero in 2002 (Ross and Lott, 2003). Location does matter for the socioeconomic impacts of drought.

Though the most recent multi-year drought to strike the West was severe, especially in terms of its impact on water resources, the two most severe droughts since 1900 remain the legendary 1930's "Dust Bowl" drought (1929–1940) and the 1950's Southwest drought (1946–1956) (Fye et al., 2003, 2004). These start and end year dates were determined by an objective method based on the duration of running sums of PDSI values (Fye et al., 2003). The two worst years of those droughts, 1934 and 1956, are shown in Fig. 2. The environmental impact of the 12-year Dust Bowl drought was certainly severe, but the great dust storms associated with it were largely a product of poor agricultural practices that exposed the subsurface soil to desiccation and wind erosion. It is hard to assign a firm economic cost to the Dust Bowl drought, which was especially severe in the northern Rocky Mountains and northern Great Plains. One indication of its economic cost comes from a paper on the effects of drought on vegetation in Montana (Ellison and Woolfolk, 1937). That report mentions that 350,000 "drought-relief" cattle were purchased by the government in 1934–35 for 38 counties in Montana at a cost of $5 million ($66 million in 2002 dollars; see Sahr, 2005). Viewed over the entire region affected by drought, Warrick (1980) estimates that financial assistance from the government may have been as high as $1 billion in 1930s dollars ($13 billion in 2002 dollars) by the end of the drought, a number that reflects only part of the total economic cost of the Dust Bowl drought. There is also no question about the immense social impact the drought had on farmers and ranchers, who were forced to flee the parched and exhausted soils of the Great Plains for better conditions elsewhere (Worster, 1979). That this upheaval occurred during the economic 'Great Depression' exacerbated the impact.

The 11-year 1950's Southwest drought was likewise extreme, with it being centered primarily over Texas and New Mexico. The environmental impact of the Southwest drought was severe, but it had less socioeconomic impact than the Dust Bowl drought because of irrigation,

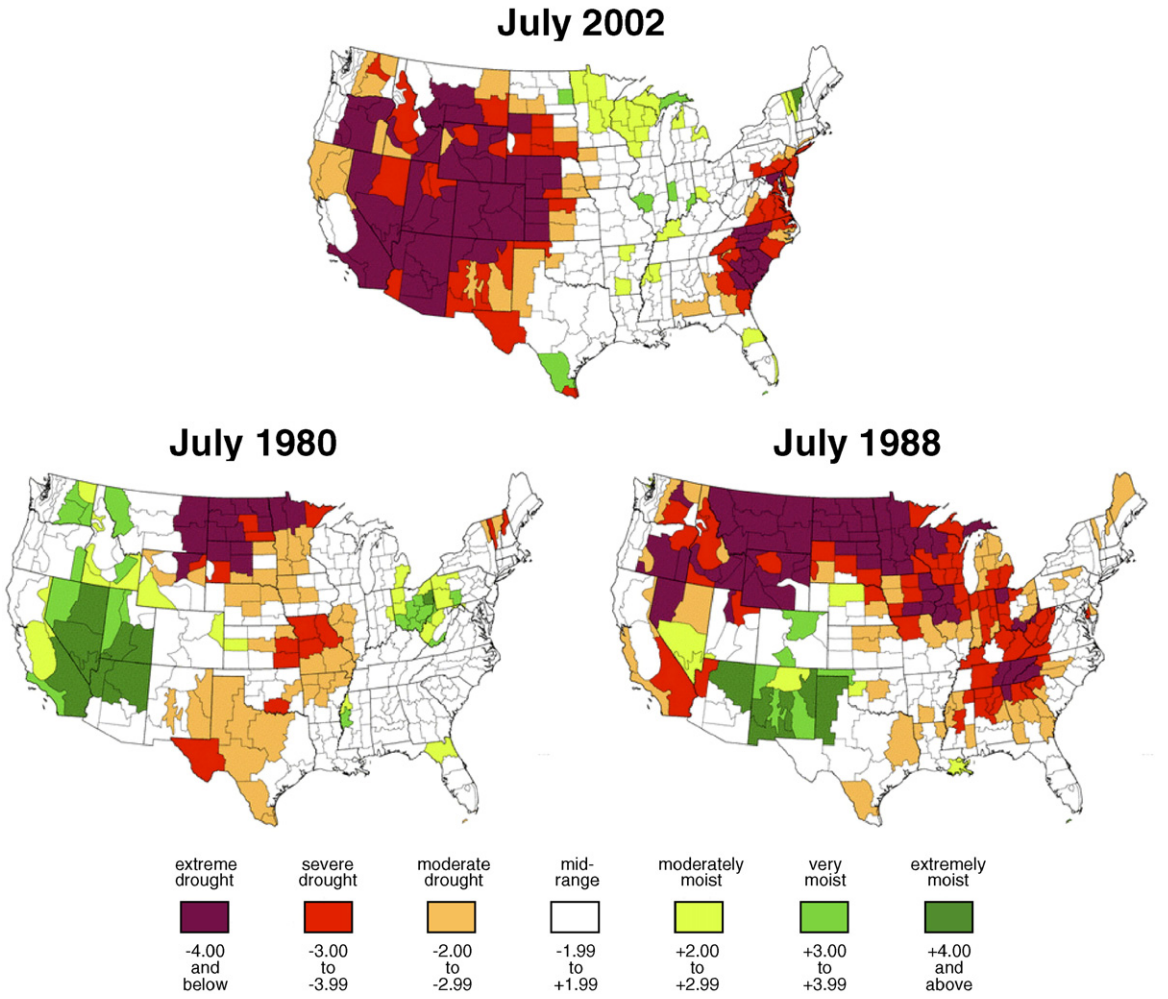

Fig. 1. Maps showing the U.S. regions most affected by drought in 1980, 1988, and 2002. The drought metric used for this purpose is the Palmer Drought Severity Index (Palmer, 1965). Note that the 2002 drought was mostly restricted to the inter-montane West, while the other two droughts were located more so in more agriculturally important regions of the Great Plains and Corn Belt. (Maps from http://www.ncdc.noaa.gov/oa/climate/research/drought/palmer-maps/).

improved agricultural practices, better governmental support, and a much stronger underlying economy. Regardless, the hydroclimatic severity and duration of the 12-year Dust Bowl and 11-year Southwest droughts tell us from even the relatively short 20th century climate records that things could get worse than the recent drought in the West that has lasted only 5–6 yr and, depending on locale, may not yet be ending.

The annual drought maps in Figs. 1 and 2 also illustrate that individual drought years are not necessarily good indicators of cumulative environmental and socioeconomic impacts. One dry year may be accommodated without undue environmental and economic harm providing that it is sufficiently offset by wetter conditions the following year. What really matters is *duration* because recovery from the cumulative damage of consecutive drought years is more difficult. Thus, while the 1934 drought year clearly exceeds the overall severity of the other years shown in Figs. 1 and 2, it was also part of a much longer sequence of drier than average years (Fye et al., 2004) that resulted in the catastrophic Dust Bowl drought.

Given the enormous environmental and socioeconomic impacts of drought over the U.S., Canada, and Mexico, it is important to develop a better understanding of North American drought, especially for multi-year events. This is a propitious time to review the state of present knowledge because of striking advances in just the past two or three years:

(1) A recent reconstruction of North American drought from AD 800 (Cook et al., 2004) creates

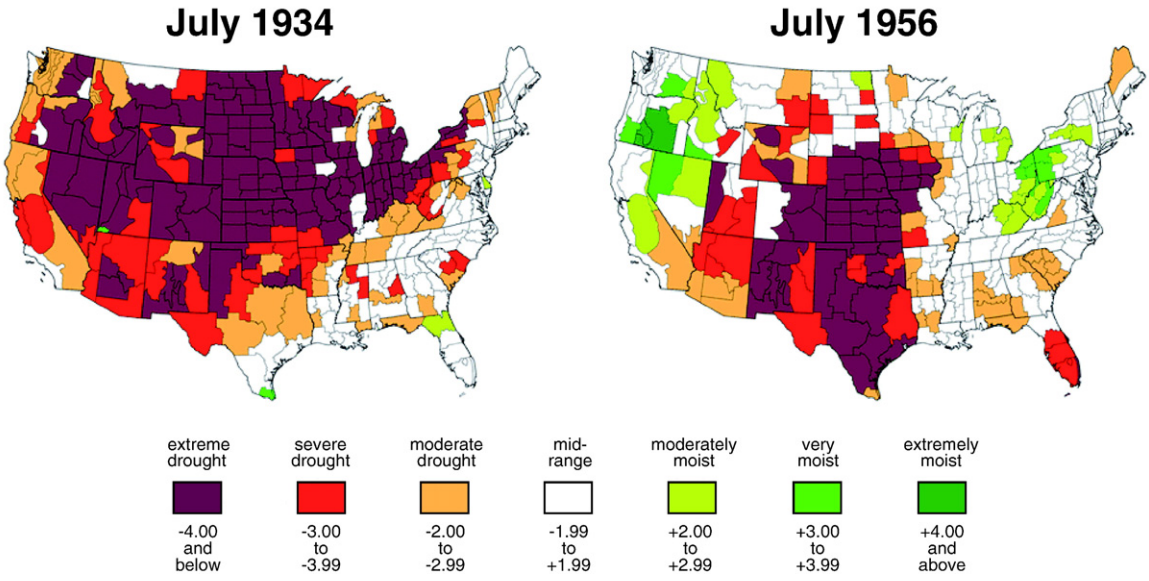

Fig. 2. Maps showing the U.S. regions most affected by drought in 1934 and 1956. These two years are part of the Dust Bowl and Southwest droughts, considered to be the worst of the 20th century. (Maps from http://www.ncdc.noaa.gov/oa/climate/research/drought/palmer-maps/).

the first annual, regionally resolved picture of more than a millennium of droughts and wet periods for most of the North American continent. It provides a context for the handful of droughts that we know of from the instrumental period (roughly, the 1850s onward) and a more complete picture of North American droughts of exceptional intensity and duration, "megadroughts" (Woodhouse and Overpeck, 1998; Stahle et al., 2000). For example, the 16th century megadrought identified by Stahle et al. (2000) is now seen to have affected large areas of North America, especially in the West and northern Mexico, and was much more prolonged than any of the 20th century droughts. The drought reconstructions also provide clear evidence for a much drier climate across the West and Great Plains during Medieval times, a drought that lasted with few interruptions for a few hundred years and which greatly taxed both hunter–gatherer and agriculturalist populations (Jones et al., 1999). Such "no analog" megadroughts are scary because the modern-day agricultural and hydrologic systems that depend upon adequate water supplies to produce and function may not have the resilience to survive much beyond the observed "worst case scenario" droughts of the past 100–150 yr, e.g., the Dust Bowl drought. The unprecedented growth of the West occurring now, with its increasing demand for water, makes this concern for the future even more serious. So, understanding the causes of these past megadroughts is vitally important.

(2) There has been rapid progress in simulating North American drought with comprehensive atmospheric general circulation models (AGCMs; Schubert et al., 2004b; Seager et al., 2005b; Herweijer et al., 2006). If global sea surface temperatures (SSTs) are specified, then important droughts such as those of the 1930s and 1950s are largely reproduced by the AGCMs. These results add important evidence about causality to the strong statistical association between certain spatial drought patterns over North America and SST anomalies over the tropical Pacific Ocean (Cole and Cook, 1998; Cook et al., 2000; Cole et al., 2002; Fye et al., 2004). An astonishing finding of this modeling work is that droughts with such major ecological and socioeconomic impacts apparently were "forced" by coherent tropical SST signals of no more than a few tenths of a degree Celsius.

(3) The modeling results have stimulated a new understanding of the mechanisms connecting tropical SST anomalies to drought over North America. The most accepted ideas about "teleconnections" rely on Rossby wave propagation to mid-latitudes. In addition, it now appears that zonally symmetric changes in the atmospheric circulation in subtropical and middle latitudes driven by the overall warming of the tropical troposphere are a means whereby the tropics influence the mid-

latitudes throughout the year, (Seager et al., 2003, 2005a,b; Lau et al., 2006, in press). Both mechanisms imply that North American droughts should be an element of a more global pattern of drought (e.g., in southern South America, parts of Europe and Asia) (Herweijer and Seager, 2006).

(4) To date the only part of the climate system that has proved to be predictable on seasonal and longer timescales is the tropical Pacific. That North American droughts – and their associated global hydroclimatic regimes – are linked to tropical SSTs raises the question of whether the SST patterns responsible are predictable on the timescales of years to decades over which a serious drought develops. The importance of tropical SSTs for forcing these global hydroclimatic regimes also makes it clear that the hydrological future of many areas will be influenced by how the tropical atmosphere–ocean system responds to anthropogenic forcing. This is currently a subject of great uncertainty in model simulations and one for which theoretical understanding is limited at best.

(5) Recent research has greatly extended our knowledge of the cultural and social impacts of past droughts (Stahle and Dean, in press). Examining these connections reveals the vulnerability of past cultures to drought, cautionary tales that especially resonate now because of the recent and perhaps ongoing drought in the West.

This paper aims to report on the current status of research into North American droughts and their consequences. It does not purport to be a comprehensive review of all work to date, much of which has been made obsolete as a result of the recent climate modeling studies. In the next section we describe the Palmer Drought Severity Index (PDSI) and explain why it is used to characterize drought. Sections 3 and 4 describe the tree-ring network that is used for drought reconstruction and the statistical methods employed. The reader who is primarily interested in the actual droughts, or is familiar with the methodology used for drought reconstruction from tree rings, may want to jump ahead to Section 5 where reconstructed drought variability since 800A.D. is discussed together with evidence for widespread medieval megadroughts. Following this, in Section 6, the social impacts of selected droughts over the last 1000 yr are discussed. This includes examples of the impacts of droughts on Indian cultures and also presents a climate background to the changing nature of European immigrants perceptions of the West through the Nineteenth Century from descriptions of the 'Great American Desert' to a later 'garden myth' that coincided with the opening of the railroads and migration of settlers into the Plains.

Section 7 presents the results of climate modeling studies (conducted at LDEO) and makes the case for droughts being forced by cold tropical Pacific sea surface temperature (SST) anomalies. The zonal mean eddy–mean flow interaction and Rossby wave teleconnection means of transmitting the signal of cold SSTs into the mid-latitudes is discussed and it is argued that North American droughts fit into a global pattern of hydroclimate regimes with elements of zonal and hemispheric symmetry. Modeling results are illustrated through a case study of the 1890s drought, the one that created a semblance of realism in the attitudes of the Federal government to settlement of the arid regions of the West. Section 8 discusses the causes of tropical Pacific SST anomalies both on decadal timescales and over the last millennium and makes the case that the medieval megadrought was caused by a shift to a more La Nina-like state during those centuries which itself was forced by relatively high solar irradiance and weak volcanism. Section 9 considers how tropical SSTs will change in the greenhouse future and how this will impact the hydroclimatic future of the West. A summary and conclusions are offered in Section 10.

2. Measuring drought variability over North America

The environmental and socioeconomic impacts of drought over North America reveal a great need for a detailed history of drought variability and extremes for real-time drought assessment studies as new droughts develop, for modeling the causes of drought, and for improving drought prediction. As a step in that direction, Karl and Koscielny (1982) used the Palmer Drought Severity Index (PDSI; Palmer, 1965), calculated from monthly temperature and precipitation data, to describe the temporal and spatial properties of drought over the coterminous U.S. back to 1895. Prior to 1895, the available climate data used to calculate PDSI were too sparse for any earlier large-scale analyses of drought across the U.S. Shabbar and Skinner (2004) developed a similar PDSI dataset for most of Canada, but only as far back as 1940 because of short instrumental climate records in the more northerly latitudes.

Dai et al. (1998, 2004) expanded the spatial coverage of PDSI on a regular 2.5° grid to cover most of North America and other global land areas, in the process extending the PDSI records back to 1870 at some locations as well. The paucity of early climate records in northern Canada and much of Mexico limits the

usefulness of these PDSI estimates prior to the early 20th century. Another gridded PDSI dataset for North America south of 50° N has recently been produced by van der Schrier et al. (2006b). It extends back to 1901 at all locations of the grid and is based on finely interpolated monthly temperature and precipitation data (New et al., 2000; Mitchell et al., 2004; Mitchell and Jones, 2005). Again, the quality of these PDSI estimates suffers in areas like Mexico with few climate records that extend back into the early 20th century.

Based on instrumental data alone, we are largely restricted to studies of variability over the 20th century. More or less, the PDSI is a commonly used metric of drought over North America and other global land areas. Other measures of drought have also been developed for use in North America and elsewhere (Heim, 2002), such as the Standardized Precipitation Index (Guttman, 1998), but are not used to the same degree as the PDSI.

So, what exactly is the PDSI? Succinctly put, the PDSI is a reflection of how much soil moisture is currently available compared to that for normal or average conditions. The PDSI incorporates both precipitation and temperature data in a reasonably realistic water balance model that accounts for both supply (rain or snowfall water equivalent) and demand (temperature transformed into units of water lost through evapotranspiration), which affect the content of a simple 2-layer soil moisture reservoir model. A runoff term is also activated when the reservoir is full. See Palmer (1965) for details. The PDSI is most commonly calculated at monthly time steps, although there is no formal restriction on its calculation at shorter or longer intervals. The PDSI has built into its formulation a Markovian persistence term of 0.897 from one time step to the next, corresponding to an e-folding time of ~10 months. This is expressed as

$$\mathrm{PDSI}_t = .0897{*}\mathrm{PDSI}_{t-1} + (1/3)Z_t$$

where Z_t is the moisture anomaly index for time t (Palmer, 1965; Wells et al., 2004). The Z index indicates how wet or dry it was during a single month without regard to past precipitation anomalies. Its combination with past PDSI means that the PDSI for a given month is a weighted function of current moisture conditions and an exponentially damped contribution of PDSI over previous months. This means that PDSI for the month of July integrates current and prior soil moisture conditions over several months. This point is important in understanding why only one month of PDSI is sometimes reconstructed by tree rings even though the trees are usually sensitive to several months of changing moisture supply during a typical growing season.

Numerous reviews of the PDSI have criticized it for its complexity and empiricism (Karl, 1983; Alley, 1984; Karl, 1986; Heddinghaus and Sabol, 1991; Guttman et al., 1992; Guttman, 1998; Heim, 2002; Keyantash and Dracup, 2002), but it remains one of the most widely used drought indices in the world and is a fundamental part of the U.S. and North American drought monitors (Svoboda et al., 2002; Lawrimore et al., 2002).

From the above brief description, it is apparent that the PDSI provides information on both relative wetness and dryness. The index itself is a dimensionless quantity that is scaled to remove, among other things, differences between regional precipitation climatologies. In principle, this allows the PDSI to be compared between, say, New York and Arizona, regions with radically different precipitation regimes. The PDSI typically falls in the range of ±4, which defines the extreme drought (−4) and extremely wet (+4) thresholds of the index (Table 1), but the range limit of the PDSI is not explicitly bounded. The frequency of events within each PDSI class in Table 1 should also be roughly comparable across regions and, therefore, independent of their regional climatologies. This means that an extreme drought (PDSI < −4) in New York should have roughly the same frequency of occurrence as an extreme drought (PDSI < −4) in Arizona. Unfortunately, this was found not to be the case using the original algorithm devised by Palmer (1965).

The spatial comparability of the PDSI across diverse climate regions has been questioned (e.g., Karl, 1983; Guttman et al., 1992) because Palmer (1965) derived coefficients used in estimating PDSI from a very geographically limited region of the central U.S. Wells et al. (2004) addressed this issue through the development of a self-calibrating PDSI (SC-PDSI) that locally adapts to the characteristics of the climate data being analyzed. This

Table 1
Classification of wet and dry conditions as defined by Palmer (1965) for the PDSI

4.00 or more	Extremely wet
3.00 to 3.99	Very wet
2.00 to 2.99	Moderately wet
1.00 to 1.99	Slightly wet
0.50 to 0.99	Incipient wet spell
0.49 to −0.49	Near normal
−0.50 to −0.99	Incipient dry spell
−1.00 to −1.99	Mild drought
−2.00 to −2.99	Moderate drought
−3.00 to −3.99	Severe drought
−4.00 or less	Extreme drought

produces better spatial comparability of PDSI over the U.S. compared to Palmer's original index, i.e., the frequency of occurrence in each PDSI class is more comparable from region to region. This improvement is especially apparent in the extreme ends of the PDSI range, a result independently validated by van der Schrier et al. (2006a,b) in Europe and North America south of 50° N. None of the other aforementioned PDSI studies (i.e., Karl and Koscielny, 1982; Dai et al., 1998, 2004), or the tree-ring reconstructions described below, is based on the SC-PDSI because it is such a new development.

3. Tree-ring reconstructions of large-scale drought variability

As indicated above (Karl and Koscielny, 1982; Dai et al., 1998, 2004; Shabbar and Skinner, 2004; Van der Schrier et al., 2006b), the climate records used to generate the large-scale PDSI datasets for North America become very sparse even in the early 20th century over significant portions of Canada and Mexico. The 100 yr of instrumental data is not enough to capture the full range of drought variability (Woodhouse and Overpeck, 1998). It is also not enough to allow drought variability to be evaluated during a time when the climate system was not heavily affected by the radiative forcing of anthropogenic greenhouse gases. Consequently, there is an urgent need to provide greatly expanded records of drought variability over North America.

The paleo-drought reconstructions needed to complement and augment the relatively short instrumental PDSI records for North America require a very special kind of climate proxy with the following properties:

1. The proxy must be highly sensitive to changes in moisture supply and evaporative stress, i.e., it must be drought-sensitive.
2. The proxy must have broad spatial coverage over North America to capture the complex spatial patterns of droughts, as revealed in Figs. 1 and 2.
3. The proxy must have well-resolved annual resolution to capture even single-year droughts.
4. The proxy must be exactly dated to allow annually resolved drought variability over North America to be compared from region to region.
5. The proxy must provide long enough records to produce estimates of past drought over the past several centuries to millennia.

Given these required properties, there is only one climate proxy that satisfies all of them: annual tree-ring chronologies. This understanding is not new, but only over the past few decades has the power of tree-ring analysis and its well developed statistical methods been brought to bear on the reconstruction of the joint space–time properties of past climate (e.g., Fritts et al., 1971; Briffa et al., 1986; Fritts, 1991; Cook et al., 1994, 1999; Zhang et al., 2004).

The development of an extraordinary network of climate-sensitive annual tree-ring chronologies that covers much of North America has now made it possible to reconstruct the joint space–time properties of drought over much of North America. This tree-ring network is the outcome of years of effort by many dendrochronologists and tree-ring laboratories throughout North America and even Europe, often working independently of each other. Because of a willingness to collaborate, share tree-ring data, and deposit tree-ring data for public access in the International Tree-Ring Data Bank (http://www.ncdc.noaa.gov/paleo/treering.html), this collective dendrochronological effort has resulted in a tree-ring network that enables the reconstruction of large-scale annual patterns of drought and wetness over much of North America for the past several centuries to millennia.

3.1. Previous large-scale drought reconstructions from tree rings

One of the earliest efforts to reconstruct drought from tree rings over a large portion of the coterminous U.S. was made by Stockton and Meko (1975). Their reconstruction of July PDSI was made for 40 variable-sized climate regions located in the western two-thirds of the U.S. using a tree-ring network of 40 tree-ring chronologies that spanned most of the reconstruction domain. Recall that July PDSI is actually a reflection of July moisture supply through the Z index plus an exponentially damped function of previous monthly PDSIs, which means that July PDSI integrates the soil moisture conditions over several months. These PDSI reconstructions covered the period 1700–1962. Later, Mitchell et al. (1979) produced PDSI reconstructions for the same 40 climate regions that extended back to 1600 using the Fritts and Shatz (1975) tree-ring network of the 65 longest tree-ring chronologies located over the western portion of the domain. In each case, the method used for reconstruction was canonical regression (Fritts et al., 1971), a method that simultaneously estimates one field of variables from another field of variables. See Cook et al. (1994) for additional examples of the use of canonical regression for reconstructing climate from tree rings.

The tree-ring network in the eastern half of the U.S. was poorly developed when Stockton and Meko (1975)

made their pioneering drought reconstructions. It took several more years of intensive tree-ring network development in the eastern U.S. before a full continental reconstruction of drought for the U.S. was feasible. Experiments in that direction were conducted by Cook et al. (1992) for the eastern U.S. to test the feasibility of producing PDSI reconstructions like those produced by Stockton and Meko (1975). However, it was not until Meko et al. (1993) that a full continental examination of tree growth patterns was made using a network of 248 chronologies. That effort did not produce explicit estimates of past drought. Rather it sought to understand how best to utilize the complex mix of tree species and drought regions over the U.S. for eventual reconstruction purposes.

Meko et al. (1993) used rotated principal components analysis (RPCA; Richman, 1986) to demonstrate that the tree-ring chronologies themselves could reproduce the same nine spatial drought factors in the U.S. identified by Karl and Koscielny (1982) from their gridded instrumental PDSI data. The tree-ring factor scores were also highly correlated in most cases with the actual PDSI data in the drought factor regions. This result was highly encouraging because it demonstrated that the tree-ring network inherently contained the spatial patterns of drought variability known to exist in the instrumental records. However, Meko et al. (1993) also showed that the uneven distribution and concentration of tree-ring chronologies over the U.S., and the geographic clustering of certain tree species as well, led to geographic distortion in the RPCA spatial factors unless the tree-ring data were first gridded. This procedure itself had its own problems, however, because of the way that different tree species in the same region might respond somewhat differently to the same climate forcing. Consequently, the direct gridding of tree-ring data distributed over a large geographic region, and with a complex assemblage of tree species, will mix differences in climate response in unclear ways that are unlikely to produce the best quality drought reconstructions.

3.2. The point-by-point regression method

Building upon the results of Meko et al. (1993), Cook et al. (1996) developed and tested a reconstruction method that successfully eliminated the previously noted difficulties associated with using a complex multi-species tree-ring network for reconstructing drought across the U.S. This method is called *Point-by-Point Regression* (PPR) (Cook et al., 1996).

PPR is the sequential, automated fitting of individual principal components regression models of tree rings to each point in a grid of instrumental climate variables, in this case PDSI. The sequential nature of PPR differentiates it from joint space–time methods used to simultaneously relate two fields of variables, such as canonical regression (Fritts et al., 1971) and orthogonal spatial regression (Briffa et al., 1986).

PPR is based on the premise that only those tree-ring chronologies proximal to a given PDSI grid point are likely to be true predictors of drought at that location, where ‘‘true” implies a causal relationship between tree rings and drought that is stable through time. The rationale behind this premise is our understanding of drought in the U.S. as a regional or mesoscale phenomenon. Consequently, synoptic-scale teleconnections between tree rings and drought, while statistically significant during any given calibration period, may not be stable through time. The local control over each regression model provided by PPR when reconstructing each grid point PDSI is not possible using the joint space–time reconstruction methods mentioned above. It also eliminates the need to grid the tree-ring data and allows each tree-ring chronology to be separately modeled as a predictor of drought.

PPR uses a *search radius* around each grid point to define the zone of local control exercised by the method in selecting candidate tree-ring predictors of PDSI. A second level of control is the *screening probability* for the correlation between tree rings and PDSI, which eliminates those chronologies from the initial candidate pool that are poorly correlated with drought. The screening is done on prewhitened tree-ring and PDSI data after the removal of short-lag autoregressive persistence (Box and Jenkins, 1976). Prewhitening effectively eliminates problems that can arise from differing levels of autocorrelation in the tree-ring and PDSI time series. It also makes statistical significance testing straightforward. The autoregressive coefficients used to prewhiten the PDSI data are also used later in PPR to add lost persistence back into the PDSI reconstructions that are initially based on the prewhitened tree-ring data. See Cook et al. (1996, 1999) for details.

Search radius and screening probability are the two primary controlling variables of PPR, but there was no *a priori* way of knowing if optimal values existed for either one. Consequently, both were tested over a broad range of values in principal components regression analysis to determine the overall best combination to use for reconstructing past drought. Each regression model was based on prewhitened instrumental PDSI and tree-ring data over a 1928–1978 *calibration period* common to all series. The pertinent statistic of interest here is the relative amount of PDSI variance explained by the

regression model, i.e., the regression R^2. Pre-1928 PDSI data were withheld from this procedure for regression model validation tests.

For testing the level of agreement between actual PDSI and model estimates in the pre-1928 *verification period*, three statistics in order of increasing rigor were calculated: the square of the Pearson correlation (RSQ), the reduction of error (RE), and the coefficient of efficiency (CE). RSQ, RE, and CE are also measures of relative variance in common between actual and estimated PDSI. All four statistics have an upper limit of 1.0, meaning perfect agreement between the actual and estimated data. However, unlike calibration R^2, which can never be negative, verification RSQ, RE, and CE can take on negative values if there is no verification of the estimates. As the square of Pearson correlation coefficient, RSQ is assigned a negative value if the Pearson r is negative. This places a lower limit on RSQ of −1.0. In contrast, RE and CE have unbounded lower limits and CE can never be more positive than RE. See Cook et al. (1999) for details. After extensive testing using the calibration and verification statistics just described, Cook et al. (1999) found that a 450-km search radius and a screening probability of 0.10 (the 90% significance level) were on average the best combination to use for reconstructing PDSI over the 155-gridpoint domain.

3.3. Drought reconstructions for the coterminous U.S.

Using PPR, Cook et al. (1999) successfully reconstructed the PDSI across the coterminous U.S. from a network of 425 tree-ring chronologies and the same instrumental PDSI grid as Meko et al. (1993). The June–July–August average (summer) PDSI season was reconstructed instead of a single month like July (Stockton and Meko, 1975). This seasonal average was chosen because the northward march of the growing season in spring caused the peak response of trees to soil moisture deficits to vary with latitude. Experiments with different months and seasons indicated that the summer season PDSI was the best compromise for reconstruction. Of the 155 grid points, only the southernmost grid point in peninsular Florida (Fig. 3A) failed to reconstruct because of a lack of suitable tree-ring chronologies in that region. The PDSI reconstructions for the coterminous U.S. covered the common period 1700–1978 at 154 grid point locations.

Extensive tests of these tree-ring reconstructions revealed that they contained the large-scale features of drought variability found in the instrumental data (Cook et al., 1999). These tests included the use of RPCA, which recovered the same nine spatial drought patterns found by Karl and Koscielny (1982) and Meko et al. (1993). This result validated the use of PPR as a method that could recover spatial information with a high degree of fidelity even though the method itself has no explicit spatial component in it. Subsequent comparisons of these drought reconstructions with those developed from the identical datasets using a completely independent method (Regularized Expectation Maximization; Zhang et al., 2004) further validated the use of PPR for reconstructing drought over the U.S.

The successful reconstruction of drought across the coterminous U.S. was a breakthrough, but it had some significant limitations. One obvious problem was that drought variability over North America does not stop at the U.S. political boundaries with Canada and Mexico. In order to study the natural patterns of drought variability over North America, those artificial constraints had to be eliminated. Another problem related to the length of these PDSI reconstructions. Although they were almost three times as long as the instrumental records, there were good reasons to believe that they were not nearly long enough to capture the full range of drought variability. Woodhouse and Overpeck (1998) and Stahle et al. (2000) each provided evidence for megadroughts in North America (i.e., droughts of exceptional intensity and duration) that predated the beginning of the reconstructions produced by Cook et al. (1999). Therefore, a concerted effort was made to eliminate the artificial political boundaries of the drought reconstructions and to extend them as far back in time as the tree-ring chronologies would allow.

4. North American drought reconstructions

In order to expand the drought reconstructions to cover most of North America, two challenges had to be overcome. First, the instrumental PDSI grid had to be greatly expanded to include parts of Canada and Mexico where the length and quality of the instrumental data was limited. The second challenge was to greatly expand the tree-ring network to enable the reconstruction of drought over as much of Canada and Mexico as possible.

4.1. Expanding the drought grid over North America

A logical choice for expanding the instrumental PDSI grid into Canada and Mexico would have been to directly use the existing 2.5° PDSI grid of Dai et al. (1998) for global land areas. This possibility was investigated, but a comparison of some of the Dai et al. (1998) grid point

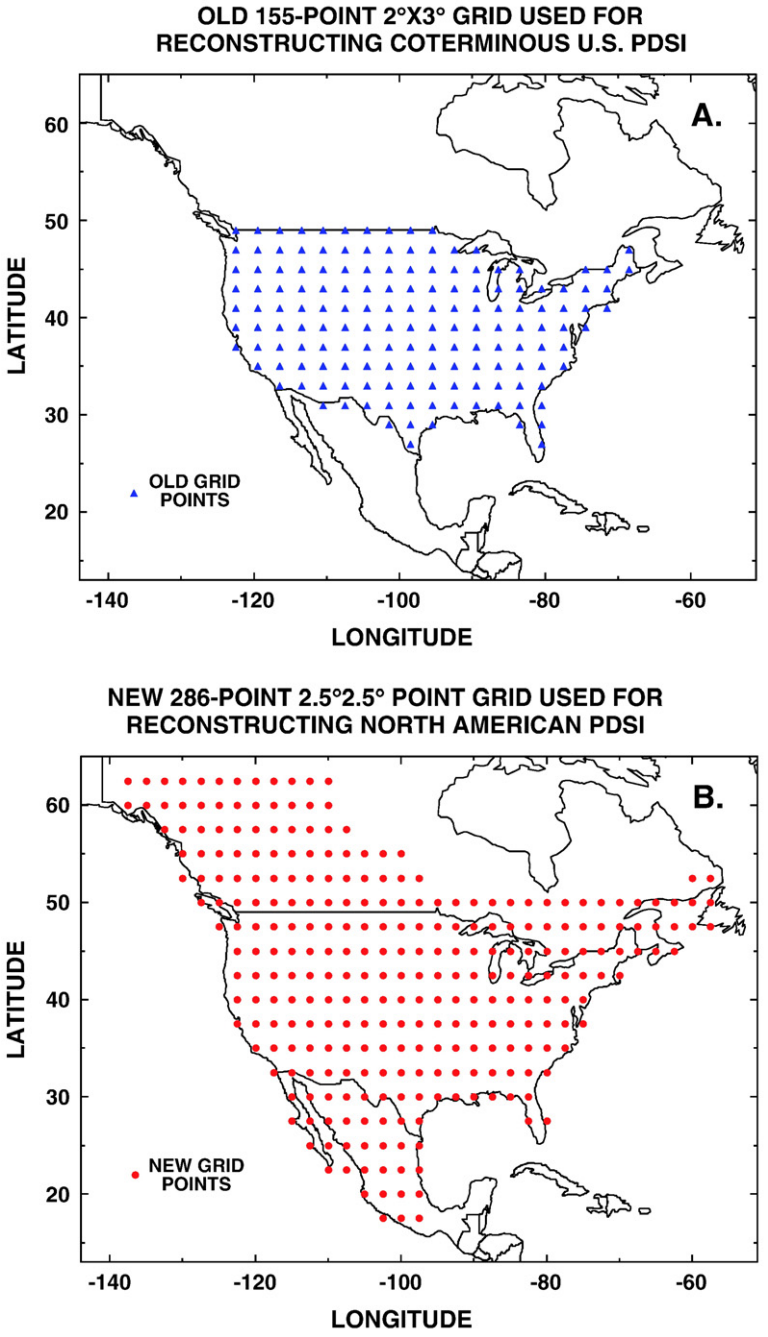

Fig. 3. The old (A) and new (B) instrumental PDSI grids used for reconstruction.

records with those closest to ones from the Cook et al. (1999) PDSI grid for the U.S. indicated somewhat weak agreement at times between the two datasets. Since the Cook et al. (1999) PDSI grid was based on the highest quality single-station USHCN monthly climate records (Karl et al., 1990), the decision was made to use these PDSI records in the expanded North American grid.

At about the same time, 131 high-quality monthly instrumental PDSI records for Canada, which all began prior to 1946, were obtained from the Meteorological Service of Canada (Skinner et al., 2001). This dataset was the basis for the interpolated PDSI records used by Shabbar and Skinner (2004) in their analyses of Canadian drought. The high-quality U.S. and Canadian

single-station PDSI records were then jointly interpolated to the same 2.5° grid as that used by Dai et al. (1998) using the same inverse distance weighted method (Cook et al., 1996). The interpolated PDSI records all began on or before 1900 in the U.S. As indicated by Shabbar and Skinner (2004), this was not possible everywhere in Canada. Therefore, areas of the Canadian grid that did not extend back to 1900 were in-filled with PDSI estimates back to 1900 using reduced-space optimal interpolation (Kaplan et al., 2000).

No similar set of high-quality single-station PDSI records existed for Mexico at the time, so the decision was made to use the Mexico portion of Dai et al. (1998) PDSI grid for that part of the North American grid. Some of the Mexican PDSI gridded records were found to be unusually erratic, with discontinuities and unrealistic extremes at some grid points, which indicated data quality problems. Those suspect PDSI grid point records were carefully edited to remove gross outliers and discontinuities. The remaining data were improved and gaps filled through the use of reduced-space optimal interpolation (Kaplan et al., 2000).

The data from the U.S., Canada, and Mexico produced a North American monthly PDSI grid composed of 286 2.5° grid points that covered most of North America (Fig. 3B). The time period common to all grid points was 1900–1990. This grid does not include Alaska, which lacks the high-quality single-station PDSI records needed for interpolation. The northern boundary of the grid in Canada was also determined by the distribution of PDSI records available for interpolation. Finally, the lack of any useful tree-ring data in the far southeastern Yucatan region of Mexico (see Fig. 3B) led to the decision not to include any PDSI grid points from that region in the new reconstructions.

4.2. Expanding the tree-ring network over North America

The second challenge was expanding the tree-ring network to cover enough of the new PDSI grid for reconstruction purposes. The tree-ring community in North America had been very active over the previous several years in developing a number of very important new tree-ring chronologies in critical areas of North America. Its willingness to share these data for large-scale drought reconstruction made it possible to rapidly expand the North American tree-ring network used here. Fig. 4A shows the tree-ring network available for reconstruction. It totals 835 annual records, many of which occupy important new regions of the grid. The new network is almost twice as large as the 425-chronology network used by Cook et al. (1999) and better fills in important parts of the U.S. in the Great Plains and Rocky Mountains. Mexico is also now well represented by the network, but significant portions of Canada are clearly under-represented. However, the results to be presented next show that the tree-ring coverage for Canada still provides useful PDSI reconstructions in a number of regions there.

Another important feature of the expanded tree-ring network is the number of new chronologies that extend back 500 or more years in the past. Fig. 4B shows a frequency histogram of starting years of the 835 chronologies, broken down into the original 425 (blue) used by Cook et al. (1999) and the additional 410 (red) in the expanded network. There are many more now that extend back into the 16th century, a period of megadrought (Stahle et al., 2000). In addition, there are a number of new chronologies that extend back before AD 1300, another time of megadrought in some areas of the West (Woodhouse and Overpeck, 1998). This enabled the PDSI reconstructions at certain grid points to be extended much further back in time into those climatically interesting times.

4.3. Extending the PDSI reconstructions back in time

The reconstructions produced by Cook et al. (1999) were originally constrained to utilize the time interval common among all 435 annual tree-ring chronologies: AD 1700–1978. In order to utilize the full lengths of the available tree-ring records for reconstructing drought, PPR was used in a nested manner whereby the shorter chronologies already used for reconstruction were dropped out and the procedure repeated using the remaining longer series. For example, if three tree-ring chronologies passed the screening probability test and their starting years were AD 1700, 1600, and 1500, then three reconstructions were generated. The first used all three chronologies and began in AD 1700, the second used the two longer chronologies and began in AD 1600, and the third used the remaining longest chronology and began in AD 1500. Each reconstruction would also have its own calibration period R^2 and verification period RSQ, RE, and CE.

In order to put these three reconstructions together into one reasonably homogeneous record back to AD 1500, it was necessary to adjust each series to account for its different level of regression R^2. Otherwise there might be an artificial trend or fluctuation in the reconstructed PDSI variance over time. This was accomplished by adding the lost variance due to regression back into each reconstruction, i.e., each nested reconstruction was rescaled to have the same variance over the 1928–1978 calibration period as the instrumental PDSI

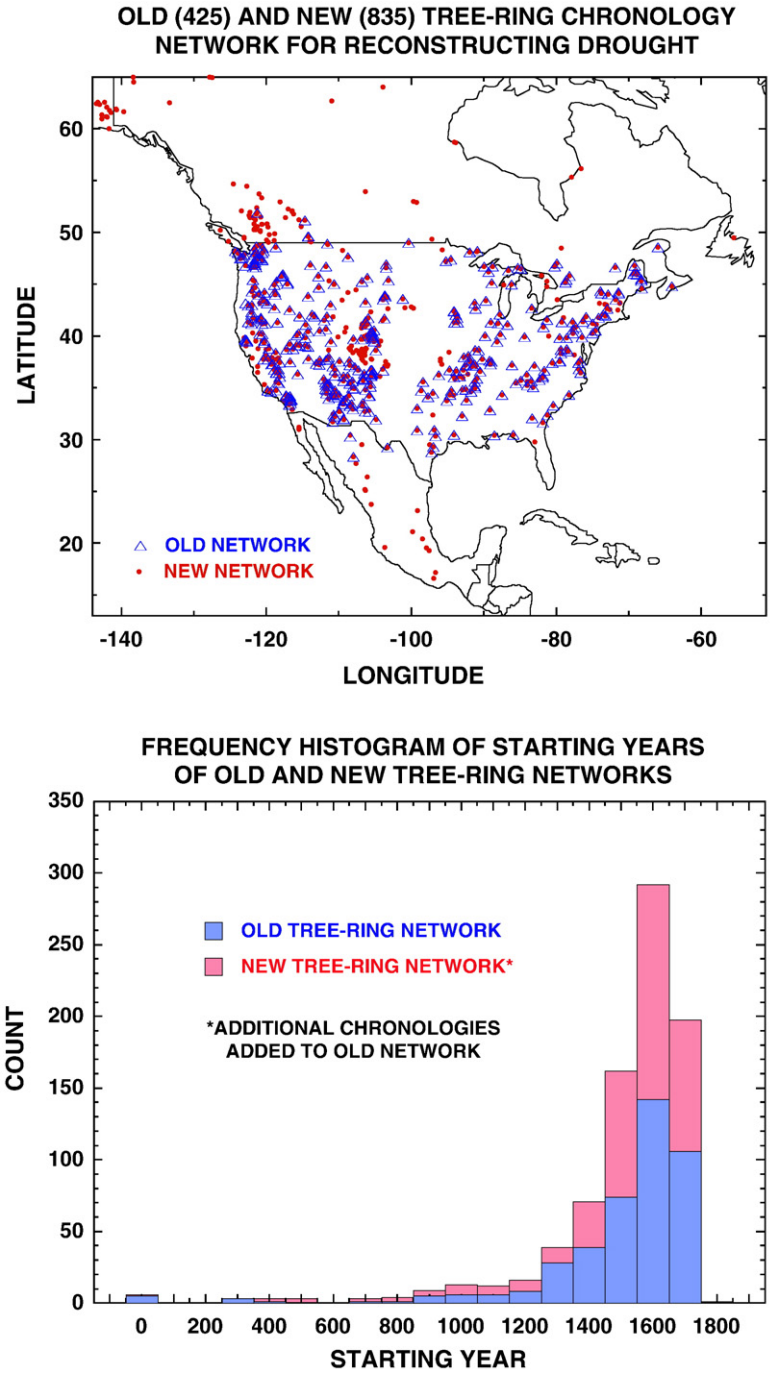

Fig. 4. The North American tree-ring network (A) used for drought reconstruction and the frequency histogram of starting years of those chronologies (B). Each shows the earlier 425-chronology network used by Cook et al. (1999) to reconstruct drought over the coterminous U.S. (blue) and the additional chronologies that make up the expanded 835-chronology North American network (red).

data. In the hypothetical example used here, this would create a PDSI reconstruction as a combination of three rescaled segments: 1500–99, 1600–99, and 1700–1978.

Fig. 5 shows an example of one reconstruction from the North American Drought Atlas that was created over the 286 PDSI grid points (Fig. 3B). The North American Drought Atlas can be accessed online at http://iridl.ldeo.columbia.edu/SOURCES/.LDEO/.TRL/.NADA2004/.pdsi-atlas.html (see also http://www.ncdc.noaa.gov/paleo/newpdsi.html for an alternative source of these

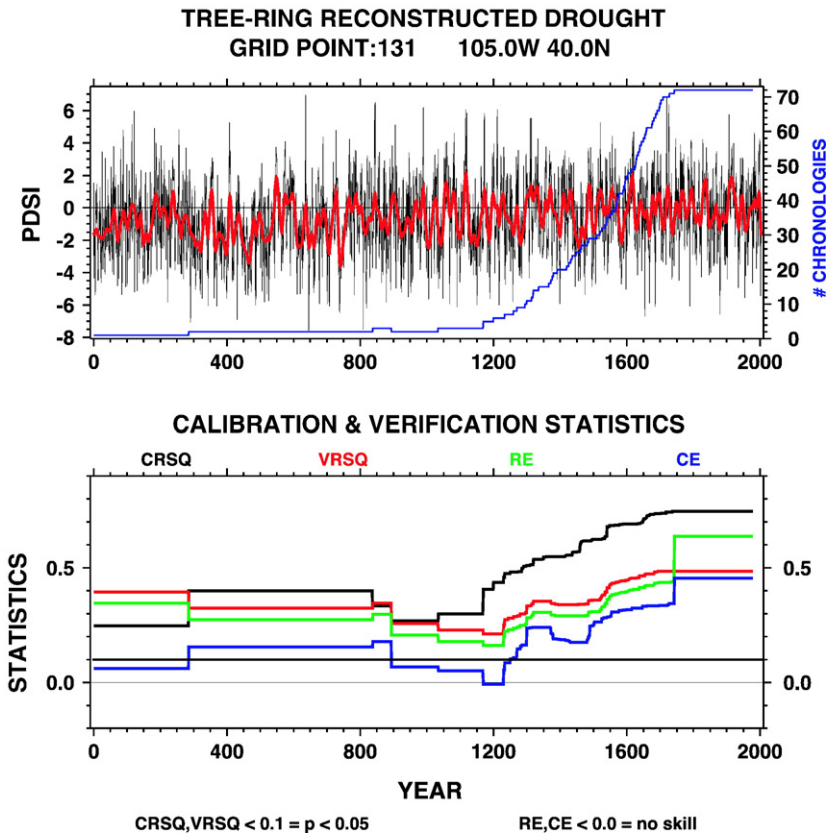

Fig. 5. An example of an extended PDSI reconstruction (upper plot in gray and red) from the North America Drought Atlas, created by using PPR in a nested manner to generate all possible length reconstructions from a suite of tree-ring chronologies with uneven starting years. The blue curve in the upper plot shows the change in the number of chronologies available back in time. As a consequence, each extension back in time has its own calibration (CRSQ, same as R^2 in the text) and verification (VRSQ, RE, and CE; VRSQ=RSQ in the text) statistics, which causes them to vary over time in the lower plot.

data). Note how the calibration and verification statistics change with time as the number of available chronologies declines. Except for one short interval centered on AD 1200 where CE<0, all of these statistics remain statistically significant ($p<0.05$) or have some detectable skill (RE>0 and CE>0) over the past 2000 yr, which indicates that this reconstruction located at a grid point in northern Colorado is useful for charactering past drought over the entire period of record. However, the sharp decline in the number of chronologies prior to about AD 1200 means that greater caution must be exercised in using the earlier portion.

5. The North American summer PDSI reconstructions

Using the 835 tree-ring chronologies in our network (Fig. 4A), PPR was applied sequentially over the 286 PDSI grid points (Fig. 3B) in a nested fashion to produce drought reconstructions of maximal length at each location. The calibration period was 1928–1978 and the verification period was 1900–1927 in every case. This process produced 286 summer drought reconstructions of the kind illustrated in Fig. 5. Many of them extend back into the megadrought epochs noted by Woodhouse and Overpeck (1998) and Stahle et al. (2000). The median starting year of the reconstructions is AD 951 and 75% of the series begin on or before AD 1380. This is a remarkable improvement over the reconstructions of Cook et al. (1999) that all began on AD 1700. The reliability of the North American summer drought reconstructions will be described next through maps of the calibration and verification statistics and their overall summary statistics.

5.1. Calibration and verification results

Calibration R^2 and verification RSQ, RE, and CE statistics have been mapped over the grid to provide guidance for which areas are reconstructed well. These

maps (Fig. 6A–D) are based on the model statistics for the most highly replicated portion of the reconstruction, i.e., that interval based on the maximum number of tree-ring chronologies used in each model. Areas with significant ($p<0.05$ or RE>0.1 and CE>0.1) calibration and verification are those shaded in all but the darkest blue color.

Each grid point must have a significant calibration R^2. Otherwise, it would not have been reconstructed. Not surprisingly, the weakest areas of calibration are located in parts of northern Canada where the tree-ring network is weakly developed. Some parts of Mexico are likewise weakly calibrated, but given the suspect quality of the PDSI data used in the Mexico part of the grid, this result may not be the fault of the tree rings alone.

The verification statistics are in general weaker than the calibration R^2, a result that was expected based upon the well known "shrinkage" of fitted relationships when applied to withheld or independent data. In general, the areas that calibrated best also verified best. This is indicated by the correlation of R^2 with each verification statistic: 0.79 for RSQ, 0.67 for RE, and 0.50 for CE. The systematic decline in correlation from RSQ to CE reflects the increasing difficulty in achieving positive values from

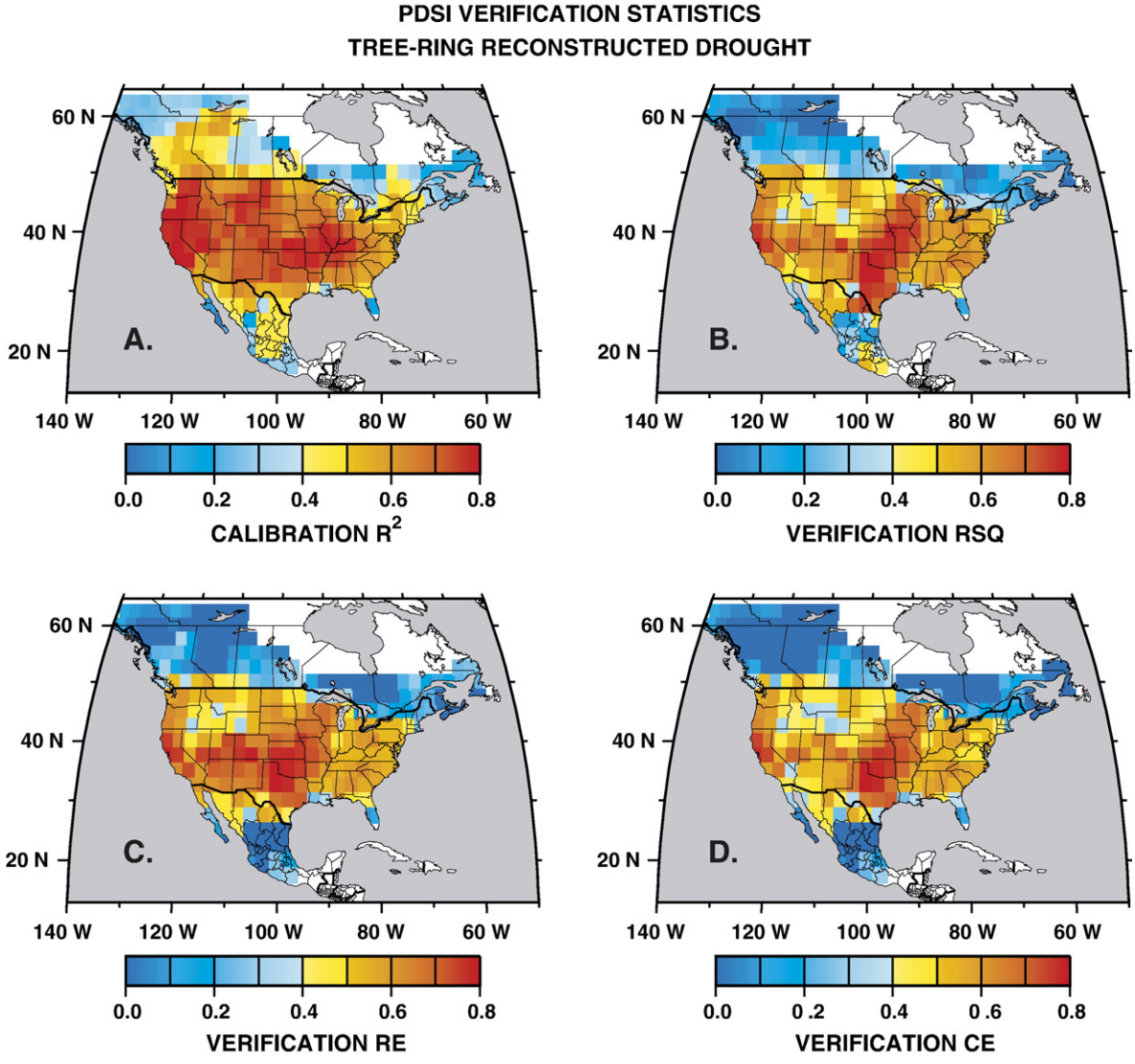

Fig. 6. Calibration and verification maps of the North America summer PDSI reconstructions. All of the grid points are significantly calibrated ($p<0.05$). Verification RSQ>0.1 ($p<0.05$) is passed at most grid points. While RE and CE>0 is often considered a sign of verification, for practical purposes, RE and CE>0.1 is probably the more appropriate threshold. This being the case, parts of northern Canada and central Mexico fail to produce positive REs and CEs.

RSQ to RE and to CE. Over the domain, there are 7 negative RSQs, 58 negative REs and 77 negative CEs. Most are located in Canada, but some are also found in central Mexico. Again, the questionable quality of the gridded PDSI data in Mexico suggests that the poor verification there may not be due to the tree rings alone.

Overall, the median R^2, RSQ, RE, and CE statistics are 0.51, 0.44, 0.42, and 0.36, respectively. These results are interesting to compare to those reported by Cook et al. (1999) for the coterminous U.S. alone: 0.55, 0.36, 0.31, and 0.22, respectively. The median R^2 in the previous study is slightly higher, but the median verification statistics are noticeably lower. Most of the improved verification in the present study probably comes about from a substantially increased tree-ring network over the coterminous U.S. (Fig. 5), which more than offsets the poor verification found in parts of Canada and Mexico.

5.2. North American drought variability since AD 951

The beginning years of the summer drought reconstructions over North America range from −1 BC to AD 1648, with most of the longer records located in the western portion of the grid. This makes a large-scale North American drought average difficult to make without introducing some geographic bias into the estimates back in time as shorter grid point reconstructions drop out. To avoid the worst of this bias, we illustrate the long-term history of North American summer drought only back to AD 951, the median starting year of the grid point reconstructions. This includes several grid points in both western and eastern North American (Fig. 7A), so there is some degree of geographic balance. The biggest missing component in the beginning is Mexico, but it is almost fully represented by AD 1380 (Fig. 7B), the year when 75% of all grid points are available.

Fig. 8 shows the average summer PDSI (MPDSI) reconstruction for all available grid points (Fig. 8A), the drought area index (DAI<−1) (in this case the percent of available grid points each year over the grid with PDSI<−1; Fig. 8B), and the percent of all grid points reconstructed for calculating these records each year (Fig. 8C). The solid black curves are the same series after applying a 60-year low-pass filter to each to highlight multi-decadal changes in drought and the upper and lower black dashed curves are 95% confidence limits based on 1000 bootstrap pseudo-samples (Efron and Tibshirani, 1986).

Not surprisingly, the MPDSI and DAI<−1 records are highly correlated with each other in an inverse sense

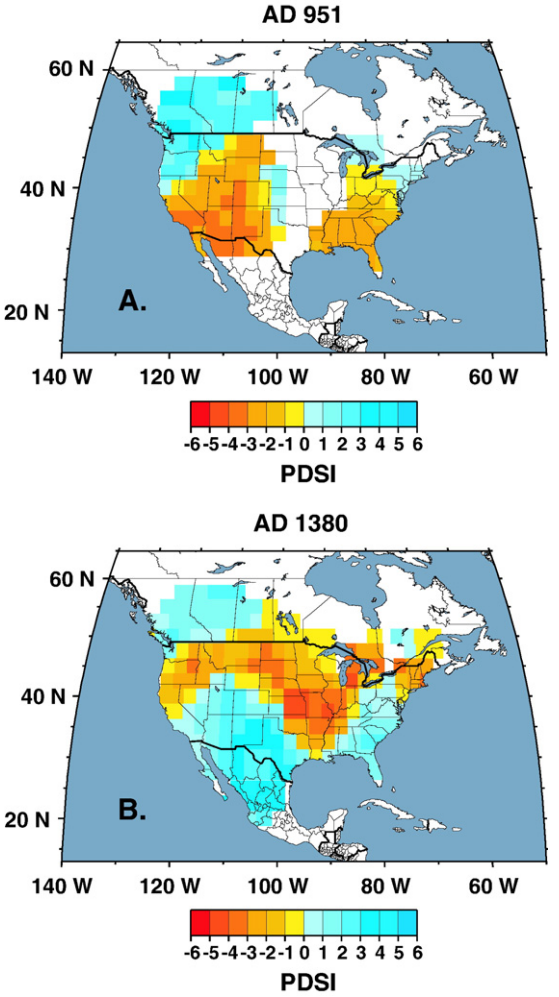

Fig. 7. Maps of reconstructed PDSI showing the geographic coverage for the years when the median (AD 951) and 75% of the grid points are reconstructed (AD 1380).

(r=−0.91). Roughly speaking, the DAI<−1 over a range of 10–50% covers an MPDSI range of ±1.0. Interestingly, both series have long-term, nearly linear trends that collectively indicate an evolution towards wetter-than-average conditions over North America. This overall trend is punctuated by significant periods of drought and wetness that in some cases lasted for several years.

The single greatest megadrought in the record occurred over AD 1140–1162, a period of 23 consecutive years of negative MPDSI across North America. The worst decade during that period was AD 1150–59 when seven of the ten years had an average PDSI across North America below −1.0. The spatial pattern of that decade of megadrought is shown in Fig. 9. Interestingly, this period of unusually severe aridity was mainly

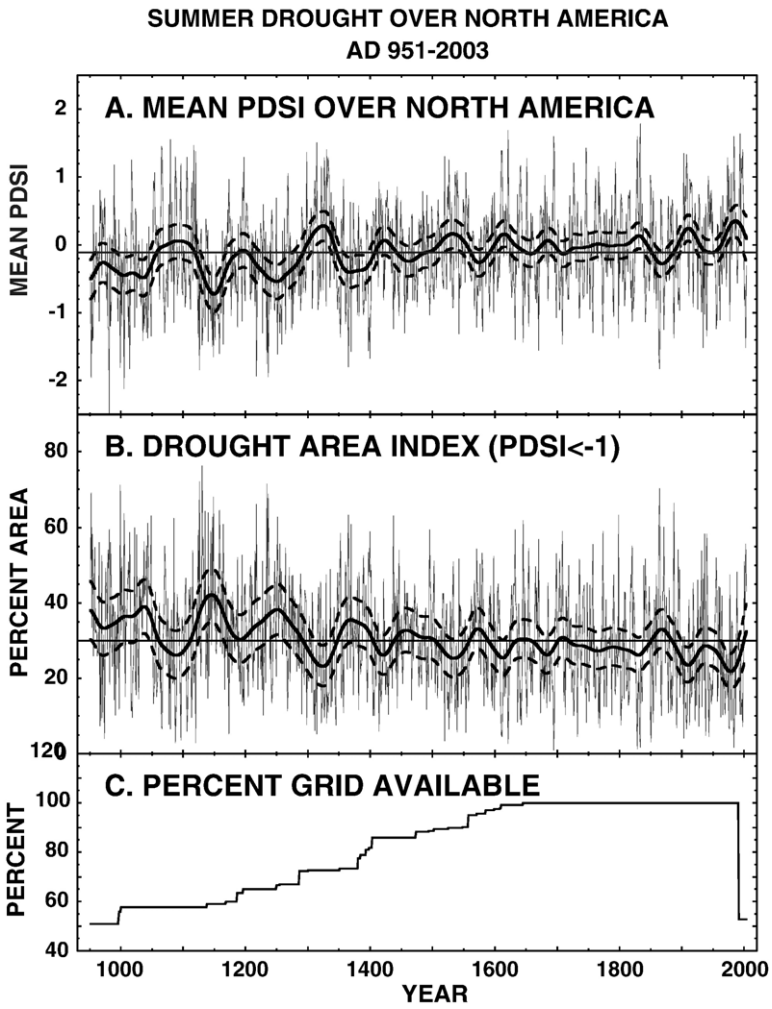

Fig. 8. Mean summer PDSI for North America (A) and percent area occupied by drought (PDSI < −1) each year (B), and the percent of the overall grid that is reconstructed each year (C). The thick solid curves are 60-year low-pass filtered versions of the annual values indicated in gray. The thick dashed curves are upper and lower 95% bootstrap confidence limits of the low-pass filtered values.

restricted to the western half of North America, with the eastern half experiencing close to normal moisture conditions on the PDSI scale (Table 1). This pattern is similar to that of the 2002 drought shown in Fig. 1, but it lasted for 10 yr. It is hard to imagine what the West would look like if the current drought with comparable severity were to last that long.

5.3. Changing aridity in the West since AD 800

Cook et al. (2004) used the North American summer PDSI reconstructions to describe long-term aridity changes in the West since AD 800 and place the current drought there in a long-term context. Fig. 10 shows the specific geographic region defined as the West (Fig. 10A) and its DAI record (Fig. 10B). On inter-annual, 20-year, and 60-year time scales of variability, the West DAI record is similar to that for North America since AD 951 ($r=0.81$, $r=0.86$, and $r=0.93$, respectively). With 60-year smoothing, the three megadrought epochs indicated for the West, centered on AD 1034, 1150, and 1253, are all similarly pronounced in the North America average. The bigger differences appear to be found in the wetter epochs. In particular, the early 20th century "pluvial" centered on 1915, which has received much recent attention in the West (Woodhouse et al., 2005), is not as pronounced in the North America average because it was largely restricted to the West (Fye et al., 2003). This again reveals an east–west contrast in moisture supply across North America, similar in form to that during the AD 1150–1159 megadrought, but with opposite sign.

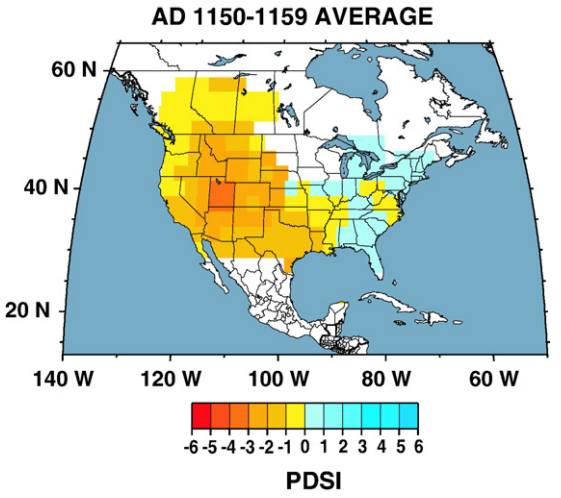

Fig. 9. Map showing the decadal mean PDSI pattern for the worst North American megadrought since AD 951. Note that it is mainly restricted to the West.

Fig. 10B also highlights the differences between 20th century drought area up through AD 2003 (boxed in yellow) and the past, especially the ~400-year period of elevated aridity from AD 900 to 1300. The mean DAI for AD 900–1300 and AD 1900–2003 are 42.3% and 30.0%, respectively, a 29% reduction in the average area affected by drought in the 20th century. This difference in average DAI is highly significant statistically ($p < 0.001$).

Further analysis of the tree-ring reconstructions (Herweijer and Seager, 2006) shows that the spatial patterns of the medieval droughts were essentially indistinct from those in the instrumental record. In addition, the PDSI extremes during the medieval droughts were no greater than for the more recent ones. While it is possible that some degree of survivorship bias in the surviving trees used to estimate severe droughts in the past has censored the magnitude of certain extreme events to some degree, it is impossible to know if this has actually occurred. Consequently, the observations made by Herweijer and Seager (2006) remain appropriate. What was so different is that, whereas the recent droughts last at most a decade, the medieval ones lasted for decades at a time and came in quick succession. The PDSI variability was, however, also similar to that of the instrumental period. The easiest way to characterize the medieval drought record is as one with variability much like today but around a mean climate that was drier. All in all this suggests that whatever currently forces intermittent droughts in the West and Plains was simply the normal state of affairs during the medieval period.

It would have immense impact on the water resources of the West in the future were modern-day conditions to revert to the drought experienced prior to AD 1300. Understanding the causes of persistent drought, and how these will be impacted by anthropogenic climate change, should therefore be a high research priority.

6. Past historic and cultural impacts of droughts in North America

The new reconstructions of summer PDSI provide sobering examples of intense decadal droughts over the past millennium that likely had severe social consequences in both the arid West and the higher rainfall areas of the eastern United States. A well documented example from the tree-ring reconstructions is the 16th century multi-decadal megadrought over the English and Spanish colonies in North America, with the gravest impacts among the native societies of Mexico where drought interacted with conquest, forced labor, and disease to contribute to one of the most catastrophic episodes of human mortality in world history (Acuna-Soto et al., 2002). In this section, we describe three such case studies of past megadroughts over North America to provide a human impact dimension to the tree-ring reconstructions.

6.1. Drought and the Puebloan society in the American Southwest

Decadal drought seems to have also played a key role in the history of Pueblo society in the American Southwest. The “Great Drouth” from AD 1276 to 1299 was famously documented by A.E. Douglass (1929, 1935) when he developed the first archaeological tree-ring chronology for Chaco Canyon, Mesa Verde, and other major prehistoric occupations across the Colorado Plateau. Hundreds of precipitation-sensitive tree-ring chronologies have been developed following Douglass’ groundbreaking research, and they confirm the multi-decadal drought of the late 13th century. These new chronologies (e.g., those indicated in Fig. 4) have been used to estimate moderate drought (summer PDSI-2.0) or worse for the entire 22-year period from AD 1276 to 1297, concentrated over the Colorado Plateau and the ancestral Pueblo cultural area (Fig. 11).

Computational models of Anasazi farming groups in time and space (so-called multiagent models; Gumerman and Dean, 2000), using surficial geomorphology and soils, palynology, tree-ring reconstructions of climatic variability and crop yields, estimated demographic conditions, and social structures for the 11th through 14th centuries in Long Valley, Arizona, indicate that the Great Drouth would have contributed to heavy

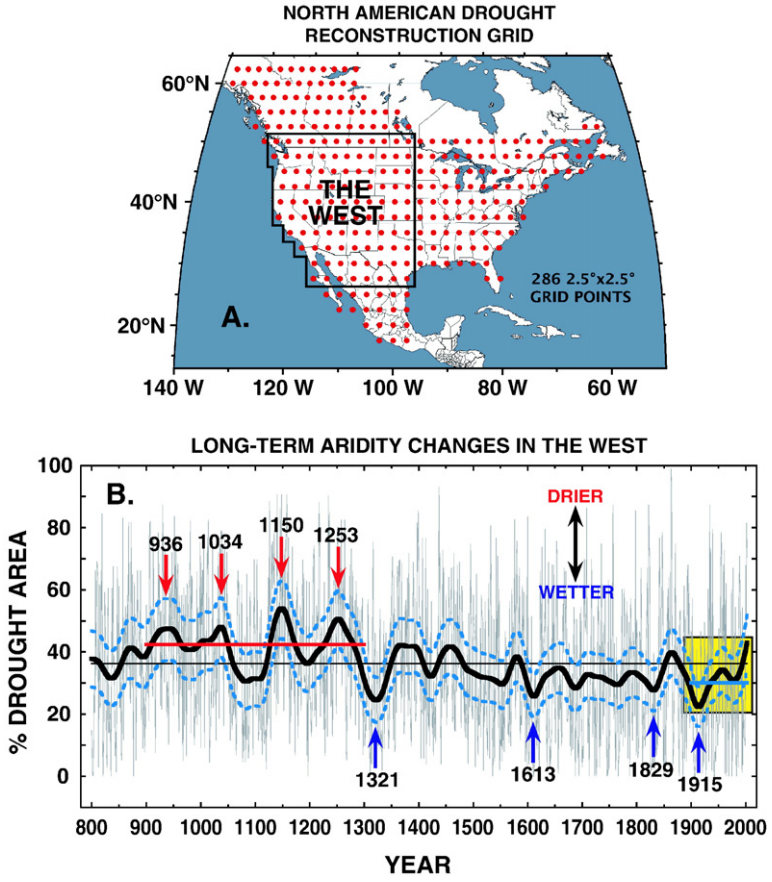

Fig. 10. Long-term aridity changes in the West (A) as measured by the percent area affected by drought (PDSI < -1) each year (B) (redrawn from Cook et al., 2004). The four most significant ($p < 0.05$) dry and wet epochs since AD 800 are indicated by arrows. The 20th century, up through 2003, is highlighted by the yellow box. The average drought area during that time, and that for the AD 900–1300 interval, are indicated by the thick blue and red lines, respectively. The difference between these two means is highly significant ($p < 0.001$).

population loss among the ancestral Pueblo, consistent with the archaeological evidence for abandonment of the region (Axtell et al., 2002). However, the modeling also indicates that the carrying capacity of Long Valley may not have been entirely depleted by the late 13th century drought, suggesting that social considerations must have influenced the decision to abandon the region (Axtell et al., 2002).

A six-year uninterrupted drought occurred over the Puebloan region and Great Plains during the mid-17th century (Fig. 11), and its impacts as described by the Spanish included famine, disease, mortality, and village abandonment (Sauer, 1980). The historical and dendroclimatic records for this 17th century drought may provide a useful analog for the social response of Pueblo agriculturalists to prolonged drought, including social changes associated with the Great Drouth of the late-13th century.

6.2. Drought during the Mississippian Phase

Severe decadal drought was not confined to the arid west over the past millennium. The tree-ring reconstructions document prolonged drought over the central and lower Mississippi Valley during the 14th, 15th, and 16th centuries, which may have contributed to the disintegration of the large complex chiefdoms of the Mississippian period. The Mississippian Phase was characterized by platform mounds, elaborate material culture, evidence for long distance trade, and a reliance on maize and native seed cultivation, fishing, and hunting. Mississippian sites are distributed across much of the central and southeastern United States, but were most spectacularly developed at Cahokia, the largest prehistoric site in the eastern United States, located in the American Bottoms south of the confluence of the Mississippi and Missouri Rivers (Pauketat, 2004).

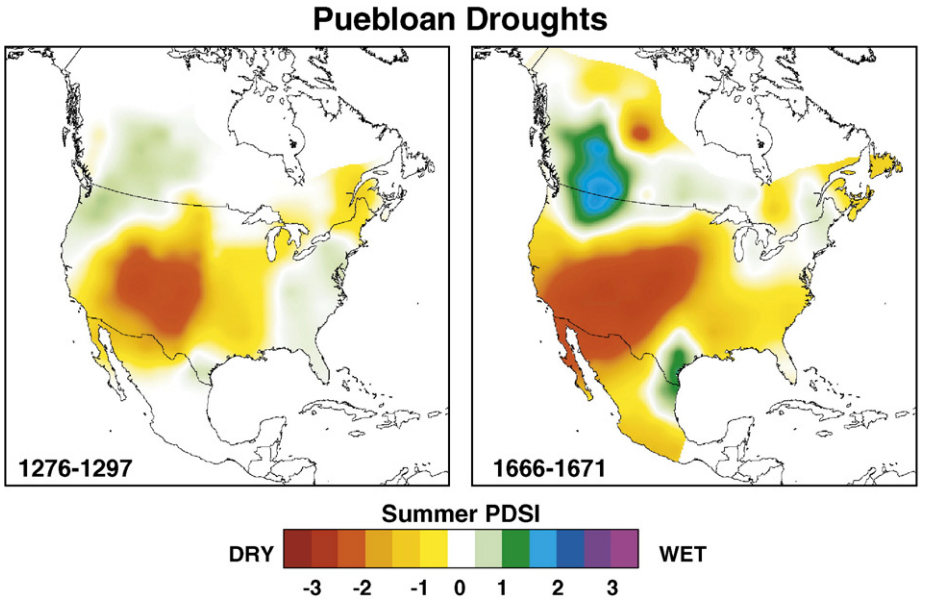

Fig. 11. Tree-ring reconstructed summer PDSI during two multi-year droughts centered over the Puebloan cultural area. The "Great Drouth" (Douglass 1929, 1935) lasted for at least 22 yr (left). The social and environmental effects of the six-year drought during the mid-17th century (right) were mentioned by Spanish archivists and may provide useful insight into the consequences of multi-year drought on prehistoric farmers in the region.

The archaeological record of development and decline at Cahokia and other major Mississippian sites has been documented with artifact analysis and radiocarbon dating (Milner, 1998). The original dating of the cultural phases at Cahokia has been shifted forward in time by a few decades in light of new results and radiocarbon calibration (Milner, 1998, p. 21). These cultural phases are believed to reflect significant changes in the human population at Cahokia, but the absolute magnitude of the population at Cahokia or in the larger American Bottoms is still very poorly known. The largest population decline at Cahokia appears to have occurred with the close of the Sterling Phase (ca. AD 1000–1200), but the final phase of occupation at Cahokia occurred during the Sand Prairie Phase, which may have persisted until ca. AD 1400 (Milner, 1998; Thomas, 2000).

Several other Mississippian mound centers were abandoned ca. 1450, including the Kincaid, Twin Mounds, and Angel sites in southern Illinois and Indiana (Cobb and Butler, 2002). The large Mississippian mound center at Spiro in eastern Oklahoma was also abandoned ca. AD 1450 (Thomas, 2000). In fact, the region from the American Bottoms south to the Ohio River and extending into central Tennessee was largely depopulated by ca. AD 1450 (Cobb and Butler, 2002). This region is centered on the confluence of the Ohio and Mississippi Rivers and is referred to as "the Vacant Quarter" (Williams, 1990; Cobb and Butler, 2002).

The abandonment of the large complex Mississippian chiefdoms by the 15th century is not well understood. Theories for chiefdom decline in the Mississippi Valley include collapse of the social organization needed to sustain the network of trade and tribute, increased warfare (which is indicated by palisade walls and skeletal evidence), deforestation and environmental degradation in the vicinity of the major population centers, flooding, and drought (Thomas, 2000; Pauketat, 2004). It is also unclear whether there was a significant population decline with the collapse of the complex chiefdoms, or whether the population was simply redistributed in smaller settlements across the region.

The summer PDSI reconstructions for the central and lower Mississippi Valley during the 14th century are based primarily on precipitation sensitive baldcypress and red cedar chronologies located in southeast Missouri, Arkansas, northern Louisiana, and east Texas (Stahle et al., 2004). These data indicate that drought prevailed in the latter half of the 14th century. Below average moisture conditions were reconstructed over the lower Mississippi Valley for 46 of 58 yr from 1344–1401 (Fig. 12). Uninterrupted moderate to severe drought was reconstructed for the two worst decades of the 14th century, AD 1344–1353 and 1379–1388 (Fig. 12). These decadal droughts were roughly contemporaneous with the decline of complex chiefdoms in

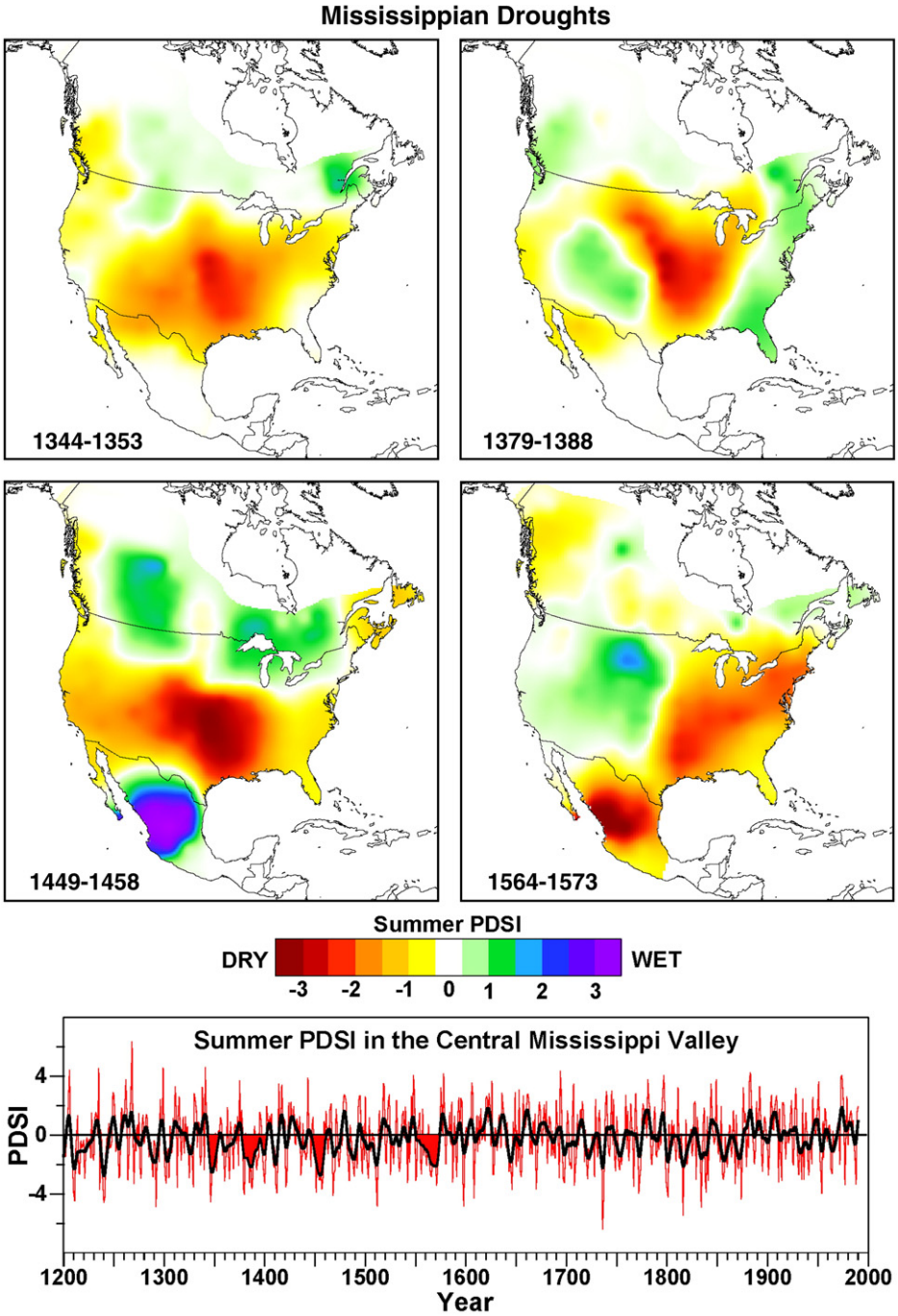

Fig. 12. Four intense decadal droughts over the central United States may have contributed to the syndrome of social and environmental change that resulted in the decline of complex Mississippian chiefdoms in the 14th and 15th centuries. The impacts of the 16th century drought (1564–1573) on native agriculturalists in South Carolina was mentioned by Spanish colonists at Santa Elena and may be relevant to earlier prehistoric drought impacts. The PDSI reconstructions for the central Mississippi Valley (time series for 37.5° N–90.0° W) indicate that the Mississippian droughts of the 14th, 15th and 16th centuries (red shading) may have been the most severe and sustained in 700 yr.

the region, possibly including the conclusion of the Sand Prairie Phase at Cahokia. Severe drought also prevailed for ten consecutive years from AD 1449–1458 (Fig. 12) and may have contributed to the depopulation of the Vacant Quarter and to the abandonment of the Spiro site.

Multi-decadal drought occurred in the Mississippi Valley and across the Southeast during the late 16th century, where it was most intense from AD 1564–1573 (Fig. 12). The agricultural impacts of this 16th century drought among the native Orista tribes of South Carolina were severe as described by the Spanish at Santa Elena colony (Anderson et al., 1995), and like the 17th century Pueblo drought (Fig. 11), the 16th century drought may provide an important historical analog to the impacts of severe decadal drought among prehistoric Mississippian agriculturalists.

The new PDSI reconstructions provide the first detailed estimates of the spatial impact of prolonged drought during this period of changing settlement patterns and increasing warfare among Mississippian chiefdoms. The widespread decadal droughts illustrated in Fig. 12 would likely have caused a sequence of poor harvests extending over a large sector of the Mississippian cultural area. The food storage capabilities of complex Mississippian chiefdoms were limited to perhaps only two years (Anderson et al., 1995), and a sequence of poor yields repeated over a few years could have been disastrous (Milner, 1998). Milner (1998) argues that widespread crop failures would have limited the ability of these chiefdoms to deploy crop surpluses from one region to another in an effort to ameliorate famine.

The time series of summer PDSI reconstructed for the confluence region of the Ohio and Mississippi Rivers (37.5° N–90.0° W) is included in Fig. 12 and indicates that the decadal droughts of the mid- to late-Mississippian period were probably the most severe and long lasting of the past 700 yr (i.e., AD 1344–1353, 1379–1388, 1449–1458, and 1564–1573; the replication and reliability of the PDSI reconstructions in the region declines before AD 1300). Climatic deterioration has been previously implicated in the decline of the Mississippian period (Thomas, 2000; Cobb and Butler, 2002), and the new PDSI reconstructions provide the first detailed temporal and spatial estimates of the most severe and sustained droughts over the central United States during the disintegration of these societies.

6.3. Perceptions of the Great Plains: The Great American Desert and the Garden Myth

The new PDSI reconstructions add interesting insight into 19th century perceptions of the American West, especially the Great Plains, and their potential for settlement and economic development. Lawson and Stockton (1981) used the earlier more limited network of tree-ring chronologies of Stockton and Meko (1975) to document widespread drought during the explorations of Stephen Long from 1819–1820, justifying the perception of the Great American Desert that arose from the expedition. We confirm their analyses with improved estimates of the severity and geographical impact of a three-year drought (1818–1820) during and just before the Long expedition (Fig. 13). The new reconstructions also indicate a severe two-year drought (1805–1806) during and just prior to the Zebulon Pike expedition (1806–1807). These extraordinary multi-year droughts must have had a severe negative impact on the vegetation cover and wildlife population levels in the Great Plains. Weaver and Albertson (1936) documented the impact of the 1930s drought on the true prairies of western Iowa, Nebraska, and Kansas, where the death of prairie plants from drought on thin upland soils ranged from 20–50% in the east to 80–95% in the western portions of their study area. Ellison and Woolfolk (1937) documented similar damage to the grasslands and woodlands of eastern Montana during the 1930s drought. The arid conditions reported by Pike and Long seem certainly to have arisen in part from the prevailing drought conditions they observed and not simply from a naïve prejudice for the wetter climates of the eastern United States.

The Garden Myth of the Great Plains, including the notion that "rain follows the plow", was largely propaganda promoted by boosters and land speculators after the Civil War to encourage settlement (Stegner, 1992). In fact, the tree-ring reconstructions indicate that the latter half of the 19th century was frequented by persistent, multi-year, droughts across much of the West (Fye et al., 2003; Cook et al., 2004; Herweijer et al., 2006). Nonetheless, three consecutive wet years occurred from the Southern Plains into the western United States from 1867–1869 (Fig. 13), and during this moist interval Clarence Thomas declared that "rains follows the plow" (Stegner, 1992, p. 298). The tree-ring data also indicate a three-year wet episode over the central Great Plains and West from 1877–1879 (Fig. 13), and soon after Charles Dana Wilber published his glowing impressions of Great Plains agricultural potential (Wilber, 1881). Both these wet periods, in the late 1860s and later 1870s, corresponded to El Niños and came on the heels of protracted La Niñas and droughts (see Section 7). The promising moist conditions of the late 1870s were soon followed by recurrent drought in the late 1880s and 1890s, corresponding to a return to a persistent La Niña-like state, and which followed the catastrophic blizzards of 1886–1887, leading to the collapse of many pioneer

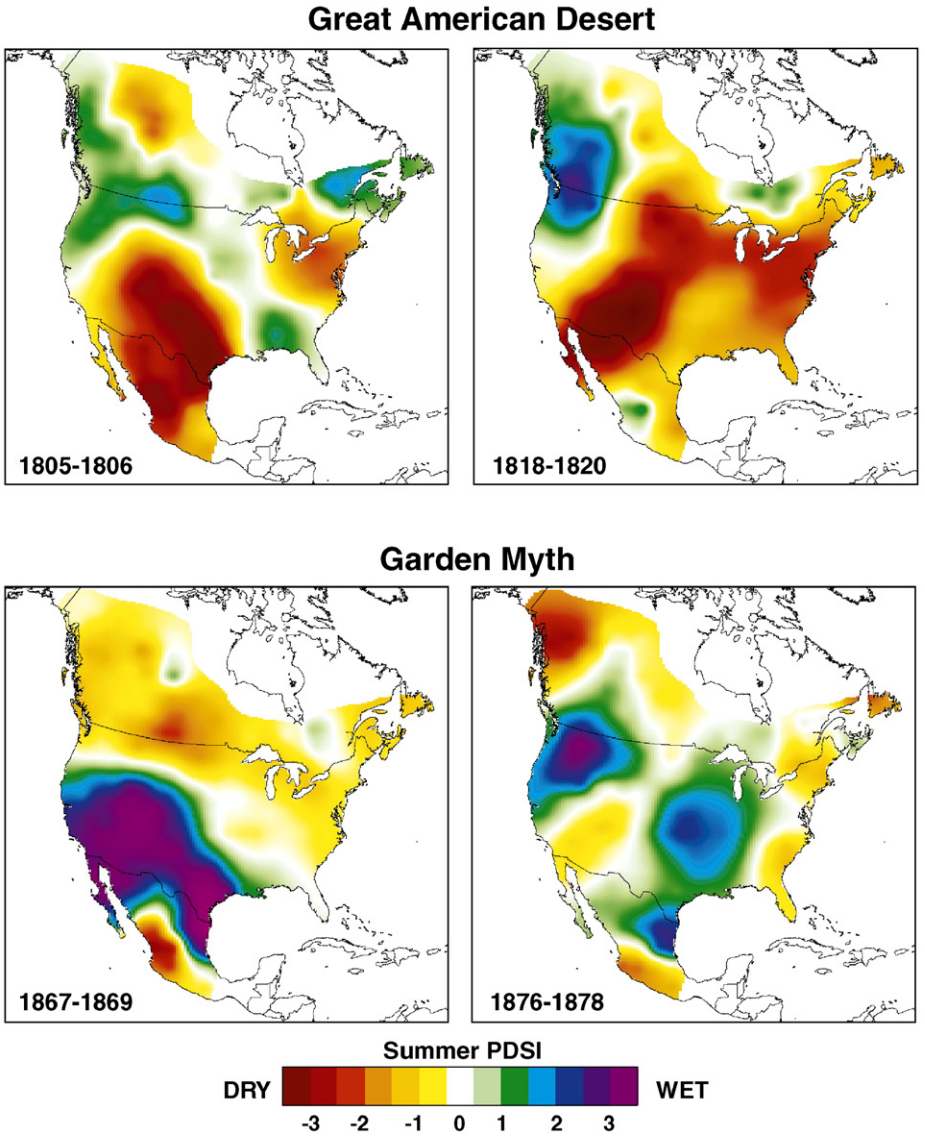

Fig. 13. Perceptions of the agricultural potential of the American West were influenced by prevailing climatic conditions (Lawson and Stockton, 1981). The Pike expedition of 1806–1807 and the Long expedition of 1819–1820 both encountered extreme drought conditions which must have contributed to their descriptions of the "Great American Desert." Episodes of above average wetness in the 1860s and 1870s may also have helped boosters briefly promote the "Garden Myth of the Great Plains," before the return of drought to the Plains in the 1880s and 1890s.

farms and ranches (Stegner, 1992; Wheeler, 1991, Herweijer et al., 2006).

The Great Plains climate is transitional between the humid east and the arid west. The instrumental and tree-ring reconstructed PDSI indicate that large portions of the Plains can become garden-like or desert-like, depending on the prevailing climatic regime. The proxy tree-ring data tell us that drought prevailed over much of the Plains during the 19th century. They further imply that modern industrial agriculture will become increasingly vulnerable to these decadal moisture regimes if the water resources of the region continue to be depleted, e.g., the High Plains Aquifer (McGuire, 2004).

7. The dynamics of persistent North American droughts

It is only in the last decade, and really only in the last few years of that decade, that progress has been made in determining the causes of sustained, multi-year, droughts over North America. This work has made clear that tropical SSTs, and in particular, tropical Pacific SSTs,

are the ultimate driver. Three developments allowed this breakthrough:

1. The first was a natural development as the first persistent drought since the 1950s spread across the northern mid-latitudes in 1998 becoming the first multi-year drought event to be well captured within the Earth and space-based instrumental record.
2. The second development was a research advance that allowed the creation of global SST and sea ice datasets using sparse, ship-based, observations. These datasets extended the record of global ocean variations back until 1856 (Kaplan et al., 1998; Rayner et al., 2003). Prior to this work research on the causes of drought proceeded like the drunk looking for his keys under the lamppost — looking for causes in SST variations where there was data, that is, in the North Pacific and North Atlantic Oceans. Namias (1983) is a good place to start down this confusing route[1].
3. The third development was a change in the attitude of climate modelers. Until very recently, model simulations of SST-forced climate variations typically began in the 1950s partly because it was only over this period that upper air data was available for verification (atmospheric reanalyses were only extended back from 1960 until 1949 a few years ago). Hence model simulations tended to begin during or after the 1950s drought and, until the last few years, end before the most recent drought. Recently, enabled by the second development above, modelers have conducted simulations that begin earlier and capture the Dust Bowl drought (Schubert et al., 2004a,b) and all six multi-year droughts in the instrumental record (Herweijer and Seager, 2006; Herweijer et al., 2006; Seager, submitted for publication; Seager et al., 2005b).

The context and dynamics of North American droughts will here be illustrated using as an example the drought that began in the late 1880s and continued until 1896. The 1890s drought came after a feverous period of migration to the West, encouraged by the railroad companies and state and federal governments (Reisner, 1986). By and large the settlement had gone along with a period of wetter than usual conditions that encouraged widespread belief that 'rain follows the plow'. Frederick Jackson Turner had announced the closing of the frontier – defined as a region of minimal population density – in 1890 but, by the end of the drought depopulation had caused its resurrection (Worster, 1985). The 1890s drought, coming on the heels of a phenomenally cold winter in 1886 that killed vast numbers of cattle, restored some sense of realism to the difficulty of settlement in the arid regions and ended the idea that sturdy settlers, working alone, would be able to transform the West.

Libecap and Hansen (2002) demonstrate the impacts of the drought on agriculture and homesteading and the extent to which the prevalent 'dry farming' doctrine was inadequate to deal with the drought. To prevent further catastrophes it became recognized that the Federal government would have to be involved and the 1890s drought can take some credit for the beginning of Federally-driven irrigated agriculture with the Reclamation Act of 1902. It is of interest to examine the meteorological origins of such an important drought and historical turning point. Results presented here for the 1890s drought are very similar to those presented for twentieth century droughts by Seager et al. (2005b) and for the two other nineteenth century droughts by Herweijer et al. (2006).

7.1. The global context of North American drought

Determining the causes of North American droughts, like most climate phenomena, is greatly aided by taking a global perspective and recognizing that these are not geographically isolated events. Hoerling and Kumar (2003), in an influential paper entitled 'The Perfect Ocean for Drought', were the first to point out that the North American drought at the turn of the 21st century fitted into a zonally symmetric pattern of mid-latitude dryness that dynamically linked the droughts in North America, the Mediterranean and central Asia.

Schubert et al. (2004b) then demonstrated that within a climate model the Dust Bowl drought of the 1930s fitted into a pattern that had not just zonal symmetry but also hemispheric symmetry. This point was amplified by Seager et al. (2005b) in a climate model simulation of the 1856 to 2000 period. To ram the point home, Herweijer and Seager (2006) used station precipitation data and climate model simulations to demonstrate that each of the six multi-year mid-latitude drought events in North America that have occurred since the onset of SST observations (1856–65, the 1870s, 1890s, 1930s, 1950s and the most recent, turn-of-the-century, drought) fitted into a global

[1] It would be an interesting topic for a historian of science to determine by how many years progress in understanding global climate variations was set back by meteorologist's habitual use of polar stereographic map projections, which inhibited the identification of tropical forcing, let alone hemispheric symmetry.

pattern with hemispheric symmetry and, in the extratropics, zonal symmetry. The drought records of the Pampas in southern South America and that of the Great Plains, in fact, share a remarkable similarity.

The global footprint of these hydroclimate regimes, and their hemispheric symmetry, suggested that the causes lay in the tropics. Indeed, Hoerling and Kumar (2003) and Schubert et al. (2004a,b) implicated tropical SSTs as the cause of the recent and Dust Bowl droughts, respectively. Going further, Seager et al. (2005b), Herweijer et al. (2006), Herweijer and Seager (2006), and Seager (submitted for publication) demonstrated that all of the six mid-latitude drought regimes were accompanied by persistent La Niña-like SSTs in the tropical Pacific, even as SST anomalies in the other oceans varied between the different events. Further, they demonstrated that this global drought history could be reproduced with remarkable fidelity in a climate model forced by the history of tropical Pacific SSTs alone.

Fig. 14 shows the observed station precipitation anomaly (from the Global Historical Climatology Network (GHCN)) and the observed SST anomaly (Kaplan et al., 1998; Rayner et al., 2003), averaged over the 1890–1896 period relative to a 1856 to 2005 climatology, together with the equivalents from the climate model ensemble of Seager et al. (2005b). The atmosphere general circulation model used is the Community Climate Model 3 (CCM3) of the National Center for Atmospheric Research. The model ensemble members were forced with observed SST anomalies in the tropical Pacific Ocean only and SST anomalies elsewhere were computed with a mixed layer ocean model — the so-called POGA-ML configuration (for Pacific Ocean–Global Atmosphere–Mixed Layer ocean). The model ensemble consists of 16 members, each integrated from 1856 to 2005 beginning with different atmospheric initial conditions on January 1, 1856. The ensemble average is shown here. The mean over such a large ensemble effectively averages over and removes the uncorrelated internal atmospheric variability in the ensemble members and isolates the part of the atmospheric circulation common to the members, that is the part that is forced by the imposed SSTs.

Station data from the 1890s is relatively sparse, and of questionable reliability, in the Americas. Nonetheless, the drought over North America can be easily seen, especially in the Plains region. The tree-ring reconstruction of the summer PDSI, which may be more accurate than the station data, is shown in the top left panel and clearly shows the drought extending into the Rockies. As described earlier, PDSI is meant to be an indicator for soil moisture anomalies. Consequently the upper right panel of Fig. 14 shows the soil moisture anomaly in the upper 1.5 m as simulated by the POGA-ML model. The model soil moisture and tree-ring reconstructed PDSI show general agreement that most of North America except for part of the Pacific coast and New England (according to the trees) were struck by drought.

Station data is very sparse in South America but there is an indication of drought in the southern regions, an area also impacted by drought in the 1930s and 1950s. Areas of Europe were also struck by drought during this period. The observed global SST anomaly of the 1890s has a classic persistent La Niña-like pattern with a broad area of colder than usual waters in the eastern tropical Pacific, warmer waters in the central and western subtropical and mid-latitude Pacific Ocean, cool waters along the Pacific coasts of the America and a cool Indian Ocean. This pattern is very similar to that which accompanies interannual La Niña events.

The middle and lower right hand panels of Fig. 14 show the drought regime from the POGA-ML model simulations. The model reproduces the North American drought and brings into relief the drought in southern South America. The tropical Americas were wet in the model – a situation hinted at in the station data – which is also typical of La Niña conditions. The model also reproduced a drought over Europe in agreement with observations. The rough hemispheric and zonal symmetry of this drought period, like the others before and after, is clear in the model.

It is also striking that most features of the global SST field during the 1890s are reproduced by the POGA-ML model as a remote response to the tropical Pacific, La Niña-like, SST forcing. This includes the cool waters along the west coasts of the Americas and the warm waters in the mid-latitude western and central Pacific Ocean in each hemisphere, a cool Indian Ocean and cool waters across most of the Atlantic Ocean. Although the modeled SST anomalies are systematically too weak – a problem we are yet to diagnose – this amount of agreement is convincing evidence that the climate regime of the 1890s, with widespread drought throughout the mid-latitudes, was a result of the persistently cold tropical Pacific Ocean of that period. It also makes clear that the SST anomalies in regions of the ocean away from the tropical Pacific, while perhaps influencing the development of the mid-latitude droughts, are not causal but are themselves a response to the tropical Pacific SSTs.

7.2. Eddy–mean flow interaction and tropical forcing of mid-latitude drought

The anomaly during the 1890–1896 period of the zonal mean zonal winds and temperature are shown in

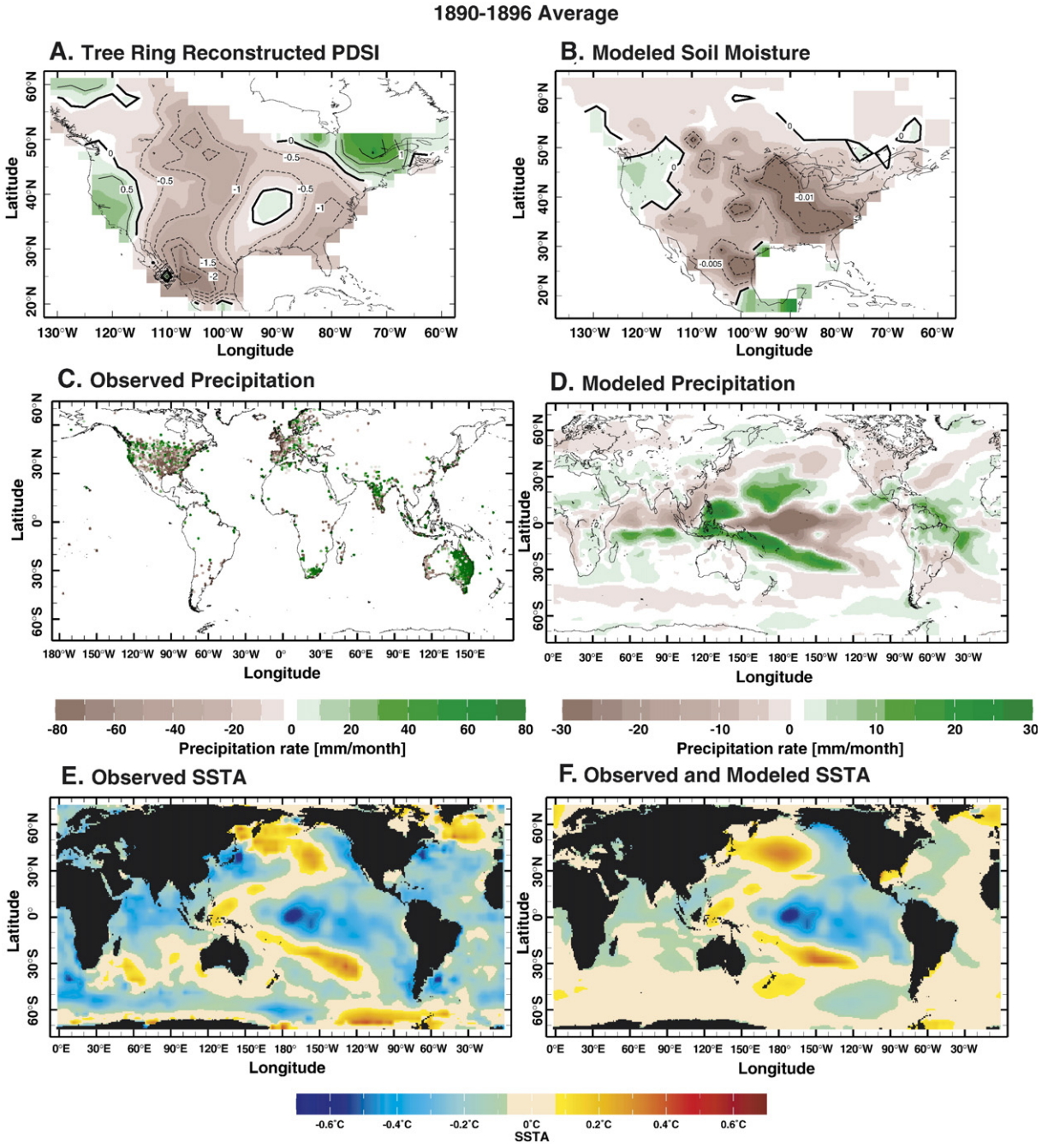

Fig. 14. Top row: the tree-ring reconstructed PDSI (left) and the modeled soil moisture anomaly within the POGA-ML ensemble (right), both non-dimensional. Middle row: the observed precipitation anomaly for 1890–1896 as derived from station data (left) and the POGA-ML simulation (right). Bottom row: the observed SST anomaly (left) and the SST anomaly from the POGA-ML model (right) which is a combination of observed SST anomaly in the tropical Pacific and computed SST anomaly elsewhere. Units are mm per month for precipitation and Kelvin for temperature.

Fig. 15, as simulated by the POGA-ML model, for both the winter and summer half years of the period. Generally the troposphere in the model was cooler during this period, a manifestation of the overall tropical Pacific warming in the Twentieth Century, but, once more, the typical La Niña-like pattern is

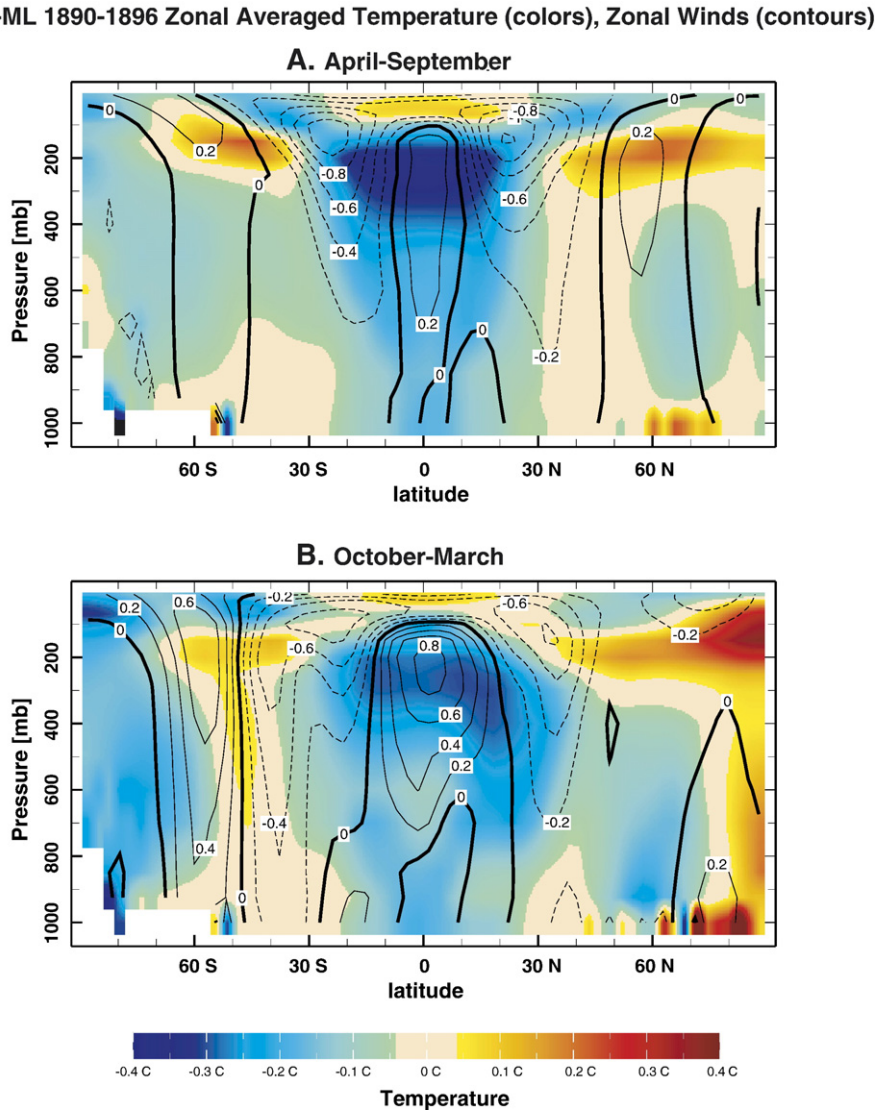

Fig. 15. Anomalies of the zonal mean temperature (colors) and zonal mean zonal wind (contours) from the POGA-ML model for the 1890–1896 period for the northern hemisphere summer seasons (above) and winter seasons (below). Units are Kelvin for temperature and meters per second for winds.

evident. There was strong cooling in the tropics with a maximum in the upper troposphere and a cooling minimum, or actual warming, in the mid-latitudes of each hemisphere. Consistent with this pattern, the subtropical jets were weaker in each hemisphere. Allowing for the overall cooler period, this is essentially the opposite of the pattern of hemispherically symmetric climate change, with tropical temperature anomalies inducing opposite signed anomalies in mid-latitudes, identified by Seager et al. (2003) as the typical response to El Niño.

How the changes in the subtropical jets impact the mid-latitude climate can be understood with reference to the zonal mean governing equations in the extratropics:

$$-f\langle\overline{v}\rangle = -\langle\overline{u'v'}\rangle_y, \tag{1}$$

$$f\langle\overline{u}\rangle = -\langle\overline{\phi}\rangle_y, \tag{2}$$

$$\langle\overline{v}\rangle_y + \langle\overline{\omega}\rangle_p = 0, \tag{3}$$

$$\langle\overline{\omega}\rangle(\langle T\rangle_p - \kappa\langle T\rangle/p) = -\langle\overline{v'T'}\rangle_y - \langle\overline{\omega'T'}\rangle_p + \kappa\langle\overline{\omega'T'}\rangle/p + R, \tag{4}$$

together with the vertically integrated moisture equation:

$$\langle \overline{P} \rangle = \langle \overline{E} \rangle - \int_0^{p_s} \left((\langle \overline{v} \rangle \langle \overline{q} \rangle)_y + \langle \overline{v'q'} \rangle_y \right) \mathrm{d}p. \quad (5)$$

In these equations the angle brackets denote a zonal mean, overbars denote the monthly time mean and primes denote the deviation from the time mean. The zonal, meridional and vertical pressure velocities are denoted by u, v and ω, T is temperature, q is specific humidity, P is precipitation, E is surface evaporation, p is pressure, ϕ is geopotential height, f is the Coriolis parameter, κ is the gas constant divided by the specific heat of air at constant pressure and R is the radiative flux convergence. Contributions to the zonal mean circulation, temperature, and precipitation by the stationary waves have been omitted for illustrative purposes but can be important.

Seager et al. (2003) detailed the way in which the changes in the subtropical jet streams impact the vertical and meridional propagation of transient eddies. The changes in subtropical jet stream and location are controlled by thermal wind balance (Eq. (2)): as the tropics cool a reduced meridional pressure gradient causes the subtropical jet to weaken. For the case of weaker jets, as during persistent La Niña conditions, transient eddies propagate less deeply into the tropical upper troposphere, instead depositing their momentum further poleward. As such, there is less poleward eddy transport of zonal momentum in the subtropical upper troposphere and more poleward transport in the mid-latitudes. The modeled anomalies of eddy momentum fluxes during the 1890s drought for the summer and winter half years are shown in Fig. 16A.

As seen in the equations, the convergence of eddy momentum flux has to be balanced by the Coriolis torque associated with the mean meridional velocity. That is, the anomalous eddy momentum fluxes induce a mean poleward flow. By continuity the induced meridional flow will force descent where there is upper tropospheric mass convergence. The subsidence is given by:

$$\langle \overline{\omega}(p) \rangle = -\int_0^p \left(\frac{1}{f} \langle \overline{u'v'} \rangle_{yy} - \frac{\beta}{f^2} \langle \overline{u'v'} \rangle_y \right) \mathrm{d}p. \quad (6)$$

By examining the eddy momentum fluxes shown in Fig. 16A (here shown just for the October through March half year) it can be deduced from this relation that subsidence (positive ω) will occur due to the first term on the right. (The β term will move the subsidence equatorward.) The modeled subsidence anomaly during the 1890s drought is shown in Fig. 16B: there is anomalous downward motion in the mid-latitudes of each hemisphere, just where expected if eddy momentum fluxes were the cause.

Downward motion forces warming due to compression. This is balanced in part by increased radiative cooling and in part by reduced transient eddy heat flux convergence (Seager et al., 2003). Note that, as is typical, the transient eddy heat flux acts diffusively, opposing a temperature anomaly created by the mean flow (see Robinson (2005) for a discussion of this). The subsidence will also lead to low level divergence and, as can be seen from the moisture equation, to a reduction of $P-E$ and, in general, a reduction in precipitation itself. This makes sense as a budget but also in a more fundamental way. Precipitation only occurs where there is ascending motion since that is required to convert water vapor into condensate. Any process, in this case transient eddy momentum fluxes, that forces descent will suppress precipitation. The details of how the moisture budget comes back into balance – whether there is reduced evaporation or moisture convergence by the mean flow or transient eddies – is less important than the fact that forced descent will suppress precipitation (Seager et al., 2005a). The changes in the zonal mean moisture budget are much the same as is shown for the 1930s and 1950s in Seager et al. (2005b): the precipitation anomalies most closely track the anomalous moisture convergence by the zonal mean flow, both in the tropics and the extratropics. In the zonal mean the convergences and divergences by transient eddies and stationary eddies largely cancel each other out. These results are not shown here for brevity.

7.3. Tropically-forced stationary Rossby waves and drought over North America

The zonal mean circulation anomalies are not the entire story however. In addition stationary Rossby waves are excited by the precipitation anomalies over the tropical Pacific (reduced precipitation and atmospheric heating at the Equator and increases off the Equator) and propagate poleward and eastward. Understanding of these waves goes back to Hoskins and Karoly (1981) and Trenberth et al. (1998) provide a useful review. The Rossby wave- or teleconnection-pattern associated with La Niñas creates an upper level anticyclone over the eastern North Pacific, a cyclone over western Canada, and another anticyclone over the southern United States. In winter these wave trains are essentially equivalent barotropic, that is they have the same sign throughout the troposphere, as can be seen by

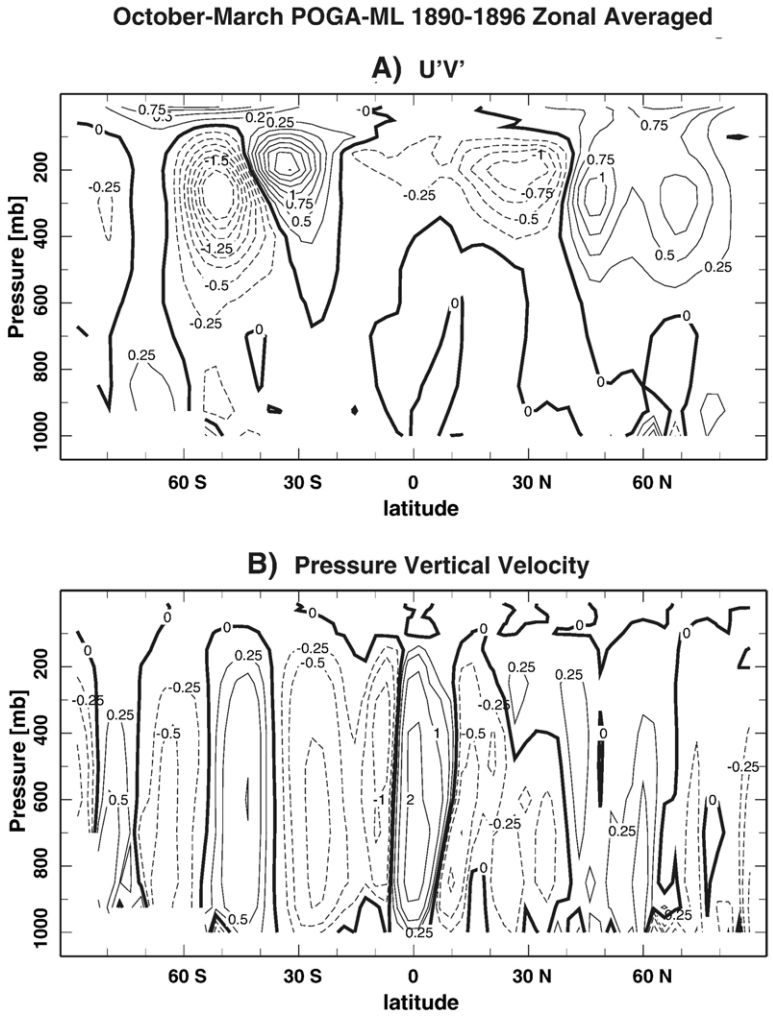

Fig. 16. The meridional flux anomalies of zonal momentum by transient eddies (top) and vertical pressure velocity (below) for the northern hemisphere winter half years as simulated by the POGA-ML model. Units are meters squared per second squared for momentum flux and Pascals per second, times one thousand, for pressure velocity.

comparing the upper level height anomalies with the lower level height anomalies in Fig. 17B.

Fig. 17A shows the upper level geopotential height anomalies over the Americas during the winters of the 1890s drought. The ridges of high pressure, expected as part of the zonal mean response to La Niña conditions, are clearly seen in the mid-latitudes of each hemisphere. In addition the Rossby wave signal over the Americas is clear with a wave train of alternating cyclones and anticyclones. The southern United States lies under a high. Also shown in Fig. 17A is the *P–E* anomaly and it is clear that this high corresponds to atmospheric moisture divergence and, hence, negative *P–E*. Thus, the zonal mean signal of mid-latitude drought is regionally intensified over North America by Rossby waves propagating from the tropical Pacific Ocean.

Fig. 17C shows that the regions of drying lie under regions of anomalous descent, just as in the zonal mean.

Fig. 17. The winter half years of the 1890–1896 drought as simulated with the POGA-ML model. The top panel shows the 250 mb geopotential height anomaly (contours) and the *P–E* anomaly (colours). The middle panel shows anomalies of 850 mb geopotential height (contours) and surface temperature (colors). The bottom panel shows the 850 mb winds as vectors and the 500 mb vertical pressure velocity and colors and contours. Units are mm per month for *P–E*, meters for geopotential height, Kelvin for temperature, Pascals per second, times one thousand, for pressure velocity and the scale for the vectors is shown at lower right.

POGA-ML October-March 1890-1896 Average

A) Precipitation-Evaporation (color), 250 mb Geopotential Height (contours)

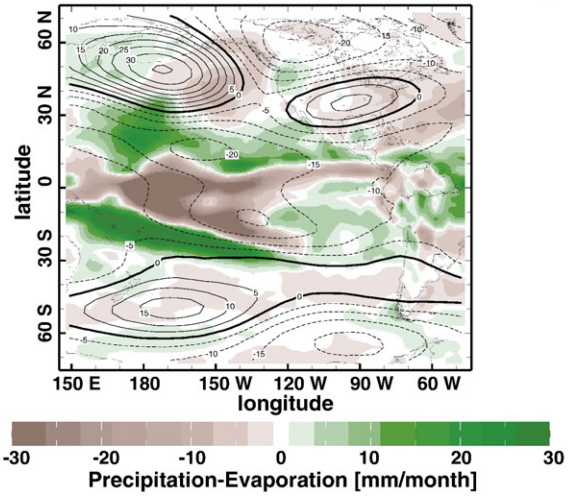

B) Surface Temperature (colors), 850 mb Geopotential Height (contours)

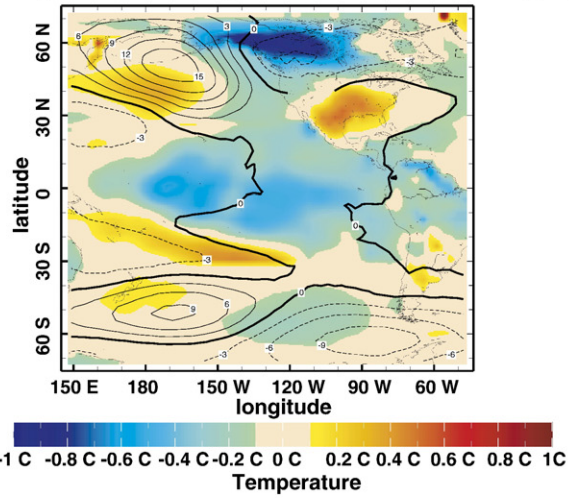

C) 500 mb Vertical Pressure Velocity (colors, contours), 850 mb Winds (vectors)

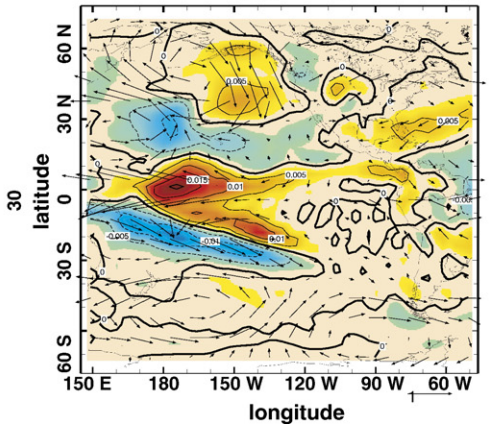

In this case however the possible causes of descent are more complex than in the zonal mean and linked into the stationary wave response. As can be seen by the low level wind field anomalies in Fig. 17C, equatorward flow induces descent. This could arise from a balance between advection of planetary vorticity by the anomalous flow and vortex compression and/or between advective cooling and subsidence warming. This is quite apparent west of the west coast of North America. It is also, in general, true over the Great Plains region during summer. In this case the equatorward flow may be caused by eddy-induced subsidence and can amplify the drought by reducing the poleward flow of moisture from the Gulf of Mexico. But the situation can be made more complex by the ability of both anomalous transient eddy fluxes of heat, and anomalous mean flow advection of mean flow vorticity, to induce patterns of vertical motion.

7.4. Summertime drought and the possible role of soil moisture and land–atmosphere interaction

It has long been thought that land–atmosphere interaction can introduce persistence into droughts as reduced precipitation lowers soil moisture, reduces surface evapotranspiration and further reduces precipitation. In this sequence the length of time for soil moisture adjustment introduces a lag and a memory. Koster et al. (2004) demonstrate that, in climate models, the Great Plains and the Sahel are the two regions of the world where there is strong coupling between soil moisture and precipitation and where land surface processes can lead to persistence. Normally the timescale is thought to be on the order of seasons rather than years.

Land–atmosphere interactions are most commonly invoked during the summer season. In the models and in observations precipitation is greatly reduced during the summer (Seager et al., 2005b). During the 1930s Dust Bowl drought winter precipitation remained normal but during other droughts winter precipitation was also reduced. In general the droughts appear to be year-round phenomena.

The model simulations analyzed provide some support for a summer land–atmosphere feedback (Fig. 18). During the summers of the persistent droughts, including the 1890s one, there are positive anomalies of *P–E* over Mexico and the southern United States. This is despite negative *P* anomalies and indicates that the surface evapotranspiration is reduced by even more with anomalous atmospheric moisture convergence stepping in to provide balance. This situation would not lead to a self-sustaining drought. Instead it suggests that negative *P–E* anomalies before the summer reduce the soil moisture and, hence, the evapotranspiration in summer leading to reduced precipitation. Since the atmospheric column becomes dry, transient eddies, acting diffusively, converge more moisture into the region. In other words soil moisture feedbacks are acting as a bridging mechanism that extends the influence of winter precipitation reductions into summer.

However this is not the only process at work in the summer. The mid-latitude ridges, related to tropical cooling, are still present in summer (Seager et al., 2005b; Herweijer et al., 2006) indicating the continued existence of atmospheric circulation anomalies forced from the tropics. It is also noticeable that, during summer, the equivalent barotropic structure of the mid-latitude circulation anomalies is interrupted over North America as surface low pressure develops over the southeast and northerlies develop to the west over the Plains. This thermal low type of pattern is suggestive of a circulation response to the change in surface and column heating as the diabatic heating by precipitation is reduced and the surface cooling by sensible heat and longwave radiation is increased. This possible circulation response, and how it feeds back into the moisture budget, is deserving of more attention.

7.5. Summary of drought mechanisms

In summary, then, the persistent droughts over North America all arose as part of the response of the global climate to persistent La Niña-like conditions in the tropical Pacific Ocean. When the waters are cool so is the tropical troposphere and the subtropical jet streams weaken and move poleward. This impacts the propagation of transient eddies such that they propagate less deeply into the tropical upper troposphere. As such there is less poleward transport of zonal momentum in the subtropics and more in the mid-latitudes. The divergence of the eddy momentum transports is balanced by the Coriolis torque, resulting in poleward flow in the upper troposphere from the subtropics into the mid-latitudes.

Fig. 18. The summer half years of the 1890–1896 drought as simulated with the POGA-ML model. The top panel shows the 250 mb geopotential height anomaly (contours) and the *P–E* anomaly (colours). The middle panel shows anomalies of 850 mb geopotential height (contours) and surface temperature (colors). The bottom panel shows the 850 mb winds as vectors and the 500 mb vertical pressure velocity and colors and contours. Units are mm per month for *P–E*, meters for geopotential height, Kelvin for temperature, Pascals per second, times one thousand, for pressure velocity and the scale for the vectors is shown at lower right.

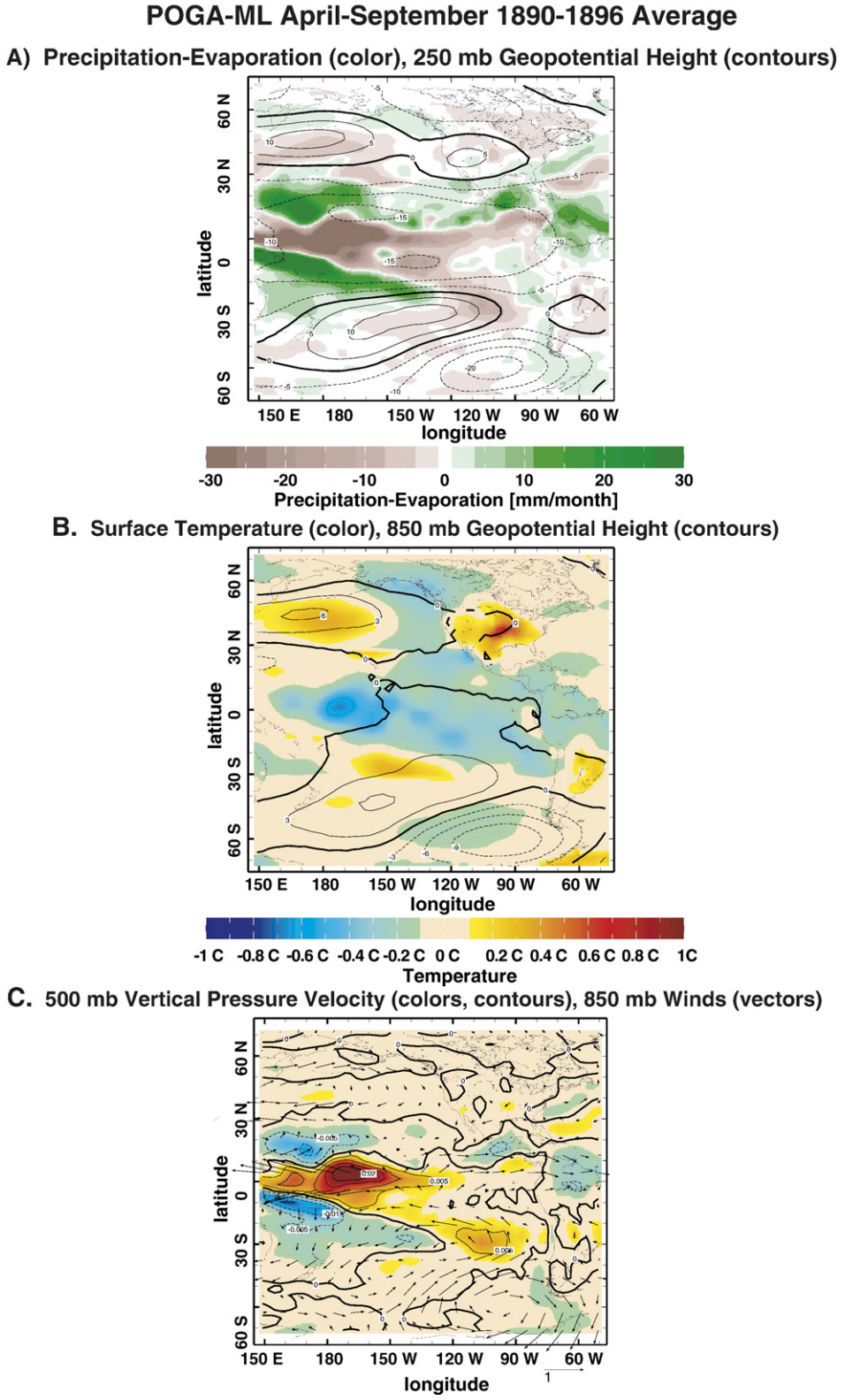
POGA-ML April-September 1890-1896 Average
A) Precipitation-Evaporation (color), 250 mb Geopotential Height (contours)
60 N
30 N
0
30 S
60 S
latitude
150 E
180
150 W
120 W
90 W
60 W
longitude
-30
-20
-10
0
10
20
30
Precipitation-Evaporation [mm/month]
B. Surface Temperature (color), 850 mb Geopotential Height (contours)
-1 C
-0.8 C
-0.6 C
-0.4 C
-0.2 C
0 C
0.2 C
0.4 C
0.6 C
0.8 C
1C
Temperature
C. 500 mb Vertical Pressure Velocity (colors, contours), 850 mb Winds (vectors)

By continuity this induces downward motion that causes warming and suppresses precipitation — at all longitudes and in each hemisphere. This zonally symmetric mechanism of tropical forcing of mid-latitude drought regimes is interrupted by stationary Rossby wave propagation from the tropical Pacific region. These stationary waves place anomalous anticyclones over North America during extended La Niña events and enhance the droughts within this region.

7.6. Possible role of Atlantic SST anomalies

The mechanism of drought generation that we have described has only involved forcing from the tropical Pacific Ocean. This is consistent with the model results presented in which adding in global SST anomalies did not lead to clearly greater skill at simulating North American droughts. In contrast using a different climate model, Schubert et al. (2004a) claim that the Dust Bowl drought was about equally forced by the cool tropical Pacific and the warm tropical Atlantic. Sutton and Hodson (2005) have also claimed that warm tropical Atlantic SST anomalies induce drying over North America. Their results are not, however, of direct relevance to the drought problem as they examined the entire 30-year period from 1930 to 1960 and compared it to the 1960 to 1990 period, whereas it is the multi-year timescale that is of most relevance to North American droughts. Sutton and Hodson also only considered the June through August part of the year whereas, as we have already stated, the droughts in general contain significant drop-offs of precipitation in spring, fall and winter as well.

There is general agreement that it is the tropical component of Atlantic SST anomalies that are important though they arise as part of a pattern with the same sign anomalies throughout the North Atlantic. Warm Atlantic anomalies go along with drought. It is often suggested that this pattern arises as a response to changes in the Atlantic thermohaline circulation (Kushnir, 1994). However there is a significant complication in that the tropical Pacific can force remote Atlantic SST anomalies and perhaps also change the strength of the thermohaline circulation. Currently there is no proposed mechanism for how tropical Atlantic anomalies force drought. This is in contrast to the two mechanisms proposed for linking tropical Pacific anomalies and North American (and global) hydroclimate, which are well evidenced in observational analyses and models and which have clear basis in dynamical theory. It could be that, during summer, Atlantic SST anomalies influence the southerly flow on the western flank of the North Atlantic subtropical anticyclone, but this is yet to be demonstrated.

The possibility of a role for the tropical Atlantic Ocean needs more investigation. The model results presented here and in the referenced papers clearly link the six droughts that have occurred since the mid-nineteenth century to cool tropical Pacific SSTs. Further the model results provide a consistent dynamical explanation. What is more, the observed droughts fit into as global pattern with hemispheric symmetry, a pattern that the tropical Pacific-forced model can reproduce (Herweijer and Seager, 2006). The hemispheric symmetry argues for a tropical Pacific cause, whereas the Atlantic mechanism relies on SST anomalies that have notable hemispheric *asymmetry*. It is hard to imagine how the subtropical North Atlantic SST anomalies could be responsible for the correlation between North American and South American droughts.

However it could be that the CCM3 model used here, while correctly representing the Pacific influence, misses an additional influence of the Atlantic Ocean. The other models that have been used to make the case for an Atlantic SST-drought link during the Dust Bowl need to be further investigated to see if the Atlantic also impacts the other five droughts. Further, it is imperative that the mechanisms that underlay such a link be determined.

8. Causes of tropical Pacific SST variability on decadal and centennial timescales

The last section makes a compelling case that the persistent North American droughts are "caused" by a particular pattern of decadal SST anomalies in the tropical Pacific that bears enough resemblance to the interannual La Niña SST pattern to be termed "La Niña-like". The obvious next questions are what causes these temperature patterns and are they predictable. A clear answer has yet to emerge.

While the principal decadal pattern of Pacific SST variability does resemble the ENSO pattern, it has broader scales and relatively greater amplitude in extra-tropical latitudes (e.g., Fig. 14C; Zhang et al., 1997). The strength of the pattern in the North Pacific led a number of investigators to regard it as primarily a northern hemisphere extratropical phenomenon, the Pacific Decadal Variation or PDO (see especially Mantua et al., 1997). In this guise it has been shown to be linked to rainfall over western North America (Gershunov and Barnett, 1998), in the same sense as the long-established link between the ENSO cycle and rainfall (Ropelewski and Halpert, 1987). An important

finding of this work is that the relationship between the PDO and rainfall is not merely the decadal average of ENSO events. This result is confirmed by the numerical experiments of Huang et al. (2005), who show that the difference between the relatively wet period from 1976 to 1998 and the preceding dry decades is successfully simulated by an atmosphere model forced only by the mean SST anomalies in the two periods; the difference is not a rectified effect of the greater El Niño activity in the later period. Consistent with the results reported in the previous section, Huang et al. (2005) also show that the tropical SSTs are the primary reason for the rainfall difference.

These model results are in keeping with observational studies showing that there are decadal variations in the South Pacific, and that these are linked to the PDO (Garreaud and Battisti, 1999; Power et al., 1999; Deser et al., 2004). Power et al. (1999), noting that "PDO" is usually taken to be centered in the North Pacific, use "Interdecadal Pacific Oscillation" (IPO) to emphasize the basin-wide nature of Pacific variability. Having the signal appear in both hemispheres implicates the tropics as a likely source, and some of this work finds a clear tropical signature in the data (see especially Deser et al., 2004).

8.1. Origins of tropical Pacific decadal variability

How much of the basin wide decadal variability is driven from coupled interactions in the tropical Pacific similar to ENSO, and how much is attributable to mid-latitude sources is an area of active research. Recall that the POGA-ML experiments described in the previous section strongly suggest that the mid-latitude SST part of the IPO pattern could be forced by atmospheric anomalies driven by tropical SST anomalies. Gu and Philander (1997) proposed that mid-latitude SST anomalies generated by anomalous heat fluxes could be subducted and carried to the equator, changing temperatures in the equatorial thermocline and then upwelled to change equatorial surface temperatures. This mechanism would complete a loop from equatorial SSTs through the atmosphere to mid-latitude SSTs and then back through the ocean to equatorial SSTs. However, careful studies of Pacific SST variations in recent decades have shown that the oceanic pathway is ineffective because the mid-latitude anomalies are diluted by mixing, especially as they move along the western boundary on their way to the equator (Schneider et al., 1999; Hazeleger et al., 2001). Still, since subduction and advection of mid-latitude waters is the source for the equatorial thermocline, this oceanic mechanism must become effective at some longer timescale.

An alternate hypothesis for Pacific variability at decadal and longer periods is that it is generated solely in the tropical Pacific by ocean–atmosphere interactions similar to those driving ENSO (Karspeck and Cane, 2002; Karspeck et al., 2004). If chaotic dynamics are dominant then there might be some hope of predicting decadal variations. Karspeck et al. (2004) and Seager et al. (2004) investigated decadal predictability in idealized experiments with the intermediate Zebiak and Cane (1987) ENSO model. They found a modest degree of decadal predictability, perhaps too modest to be of practical value. Since this was in idealized experiments, it overstates the ability to predict the real world even if the dynamics of the simplified model correctly captures the dominant dynamics in nature. If the random intrusions of mid-latitude systems or the random perturbations of intraseasonal and other tropical "noise" are more important in nature than in the model, then the predictability is smaller still. At this point the issue of predictability has barely transitioned from the issue of model predictability to real world predictability with data assimilation. The origins and predictability of decadal variability of the tropical Pacific Ocean remains a fundamental research frontier. Any multi-year predictability of North American droughts will require successful multi-year predictions of tropical Pacific SSTs.

8.2. Tropical Pacific SSTs over the last millennium

All the hypotheses described thus far rely on interactions internal to the earth's climate system. Another possibility is that the variations are forced externally by solar variations and changes in volcanic aerosols. The perennial problem with solar-climate connections is the very small size of the solar forcing signal, but because the amplitude of the decadal SST anomalies responsible for major droughts is so small (viz. Fig. 15), the solar option cannot be dismissed.

To explore this issue further, we begin with the millennium long record of drought in the west shown in Fig. 10. The first question to be answered is whether there is any evidence that the tropical Pacific SST-drought relation seen in the past 150 yr – the period of instrumental data – holds for the more extreme and extended droughts of this longer period. In this period we must rely on paleoproxies for SST information as well as for drought. The principal proxies able to resolve decadal variations are tree rings and isotopic analyses of corals. The tree rings relevant for tropical Pacific SSTs are primarily proxies for precipitation in places where the influence of ENSO and the IPO are strong, and so necessarily build in the modern relationship between

ENSO or IPO and drought. A true test of the SST-drought relationship can use only corals as a proxy for SSTs. Evans et al. (2002) obtained measures of tropical SSTs from corals at multiple sites, but since there is only a single coral head at each site, the records go back no more than a few hundred years. Cobb et al. (2003) overlapped shorter segments of fossil coral in a manner similar to the way tree-ring time series have been spliced together from individual trees. The result is displayed in Fig. 19. Palmyra (6° N, 162° W) is in a prime location to provide an ENSO proxy, and Cobb et al.'s $\delta^{18}O$ record from modern corals correlates with the NINO3.4 (120° W to 170° W, 5° S to 5° N) SST at $r=-0.84$ in the ENSO band. In other words, this coral proxy series correlates as well or better than any two commonly used ENSO indices (e.g. SOI, NINO3, NINO3.4) correlate with each other. It is likely that the $\delta^{18}O$ signal primarily reflects rainfall and so correlates better with NINO3.4 (and NINO3) than with local SST (see Evans et al., 2002). It also appears that the $\delta^{18}O$ signal is a good proxy for decadal SST.

The Cobb et al. record, taken together with the drought record of Fig. 10, appears to verify the modern relationship between SST and drought. SSTs in the eastern Pacific are low (La Niña-like) in the period circa AD 1200 when severe drought prevailed in the west, and high in the 1600s, during the Little Ice Age, when the west was wetter.

Fig. 19 also displays the mean of a 100-member ensemble calculated by forcing the Zebiak–Cane model with a slightly updated version of the Crowley (2000) solar and volcanic forcing; for details see Mann et al. (2005). There is general agreement that much of the ENSO variability is generated in ways internal to the climate system, either by chaos or noise, so we cannot expect even a perfect model to agree in detail with the single realization present in the observational record. Insofar as ENSO variability is forced, then it is possible for values averaged over a number of ENSO events to have similar features in different realizations. Indeed, Fig. 19 shows, for both model and data, cold SSTs in the mean in the late 12th–early 13th centuries, moderate SSTs in the 14th–early 15th centuries, and warm SSTs in the late 17th century. In all three cases the means of the observations and the model ensemble are consistent within the ensemble sampling distribution (dashed lines

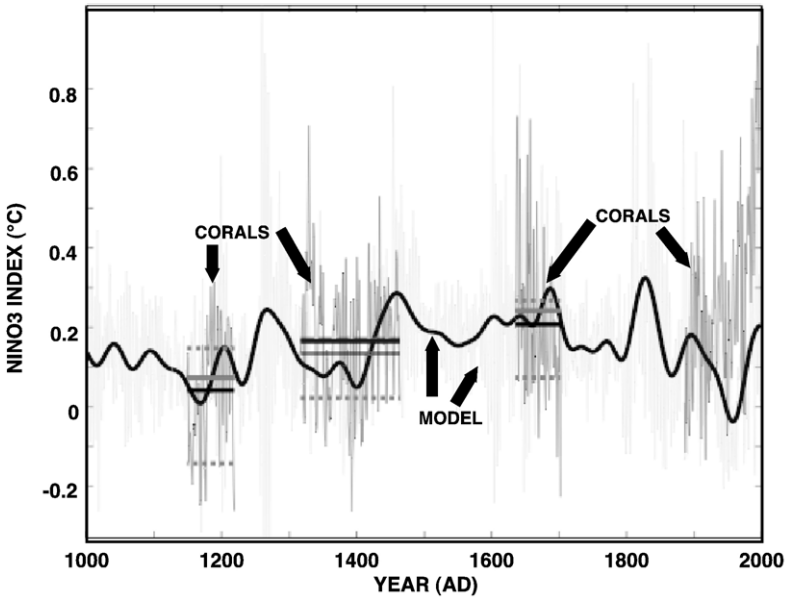

Fig. 19. After Mann et al. (2005). The annual mean NINO3 response of the Zebiak–Cane model to the combined volcanic and solar radiative forcing is compared with reconstructions of ENSO behavior from Palmyra coral oxygen isotopes. The model is run over the interval AD 1000–1999; the coral reconstruction, shown as darker grey curves, is available only for the 4 intervals shown. The continuous faint grey curve is the annual mean model NINO3 anomaly (in °C relative to the AD 1950–1980 reference period) averaged over a 100 member ensemble. Despite the averaging considerable variability remains, largely due to the influence of volcanic eruptions. The heavy black line shows 40-year smoothed values of model NINO3. The coral data (darker grey curves) are scaled so that the mean agrees with the model (see Mann et al, 2005 for details). Thick grey lines indicate averages of the scaled coral data for the three available time segments; the thick black lines are the ensemble-mean averages from the model for the corresponding time intervals. The associated inter-fourth quartile range for the model means (the interval within which the mean lies for 50% of the model realizations) is also shown (dashed grey lines). The ensemble mean is not at the center of this range, due to the skewed nature of the underlying distribution of the model NINO3 series.

on Fig. 4). Moreover, the late 17th century warmth and the 12–13th century cold are well separated within the distribution of states from the model ensemble runs: one would expect the later period to be warmer than the earlier one in roughly 7 out of every 8 realizations. Assuming these statistics, which are derived from an ensemble of model runs, apply to reality, we would expect nature's single realization to be warmer in the later period with close to a 90% probability. In both data and model there is also a systematic difference in the strength of the ENSO cycle in the two periods with more (less) ENSO variability going with a warmer (colder) mean SST in the eastern equatorial Pacific.

Due to both greater solar irradiance and fewer volcanic eruptions, the late 12th–early 13th centuries is a time of greater heating compared with the centuries since up until the last decade or two. This period is sometimes referred to as the "Medieval Warm Period", especially in studies based on data from Europe. The late 17th century, during the Little Ice Age, is a time of reduced solar radiance and more volcanic eruptions (Crowley, 2000; Jones et al., 2001). The model and data agree on a counterintuitive result: the eastern equatorial Pacific is colder when the heating is greater and visa versa. This may be understood as follows (Clement et al., 1996). If there is a heating over the entire tropics then the Pacific will warm more in the west than in the east because the strong upwelling and surface divergence in the east moves some of the heat poleward. Hence the east–west temperature gradient will strengthen, so the winds will also strengthen, so the temperature gradient will increase further – the Bjerknes (1969) feedback – leading to a more La Niña-like state.

This chain of physical reasoning is certainly correct as far as it goes, but the climate system is complex and processes not considered in this argument might be important. Perhaps cloud feedbacks play a substantial role. In a time of enhanced solar heating, the oceans should generally warm everywhere, including the subduction zones of the waters, which ultimately make up the equatorial thermocline. This might mean that the upwelled waters would warm, though, as discussed above, this mechanism does not seem to have influenced the changes observed in the past few decades. In any case, the observational evidence is that times of greater heating are times when the tropical Pacific is more La Niña-like, and the agreement between the data and the simulation with the simplified Zebiak–Cane model supports the idea that the Bjerknes feedback is dominant. Future research, especially experiments with more complex models, will doubtless clarify the mechanisms.

8.3. Uncertainties in the climate forcing over the last millennium

A more problematic issue is the great uncertainties in the solar and volcanic forcing. The size of past volcanic eruptions is inferred from proxies, primarily volcanic ash in polar ice cores (e.g., Crowley, 2000). Converting the proxy records into a radiative impact requires some form of extrapolation from the few well observed volcanic eruptions in recent times, such as Pinatubo. There is no sure way to do this. The solar forcing is at least as uncertain. Reconstructions rely on sunspot observations for recent centuries, and on paleoproxy records of cosmogenic nuclides for the longer record. The latter are directly influenced by changes in magnetic flux from the sun, not changes in irradiance. A relationship between the two must be created by extrapolating from the short period of instrumental observations, a period dominated by 11-year solar cycles which have less variation than that implied by the proxies for past centuries. The values used in the model experiments fall somewhere in the middle of values appearing in the literature, but are higher than the most recent estimates (Lean et al., 2002). Since the SST response to this forcing is just at the magnitude of the drought patterns of recent times, any reduction in the estimate of irradiance forcing makes the sun an implausible cause of the drought-inducing SST anomalies. Further, Lean et al. (2002) claim that there may not be a systematic relationship between changes in irradiance and those in magnetic flux. So while there is a reasonably convincing empirical correspondence between proxies for solar output and tropical Pacific SSTs, the great uncertainties in solar irradiance forcing raise doubts about explanations of these SST variations as responses to solar forcing.

We saw that the Cobb et al. (2003) proxy data shows cooling in the eastern equatorial Pacific at times in the past when the global climate warmed due to increased solar radiation or reduced volcanism, a result reproduced in the modeling study of Mann et al. (2005) and explained by the Bjerknes feedback. However, this same relation does not appear to hold for the 20th century, when radiative forcing and global temperatures increase. (Crowley, 2000 found the greatest disagreement between global mean temperature and a model forced by solar, volcanic and greenhouse gas variations in the early 20th century.) Perhaps this change in behavior is due to the impact of atmospheric aerosol or perhaps there is something missed in our argument when the radiative increase is due to increased greenhouse gases. Another possibility is suggested by Fig. 20, which updates Cane et al. (1997) to show the temperature trend

from 1900 to 2000. There is no change in the eastern central Pacific, but the strong warming in the west means that the east–west SST gradient significantly strengthens over the century — as would be expected from the Bjerknes feedback (Fig. 20, bottom panel). It may no longer be safe to infer the basin wide tropical Pacific SST pattern from the eastern end alone.

9. Tropical Pacific SSTs and North American drought in the greenhouse future

As has been shown, precipitation over North America is highly sensitive to tropical Pacific SSTs. Consequently the hydrological future of the American West will, at least partially, be determined by how tropical Pacific SSTs respond to rising levels of greenhouse gases. Predictions of future tropical Pacific SSTs rely on models. We would prefer that the models demonstrate the ability to simulate the defining features of the ENSO cycle with some skill. Unfortunately, most of the comprehensive Coupled General Circulation Models (CGCMs) fall short. AchutaRao and Sperber (2002) reviewed the simulations of ENSO in 17 CGCMs that were part of the Coupled Model Intercomparison Project (CMIP). Most of the model El Niños were too weak and markedly in the wrong location. Five of the models were judged to "represent well the Walker circulation anomalies, the warming and enhanced rainfall

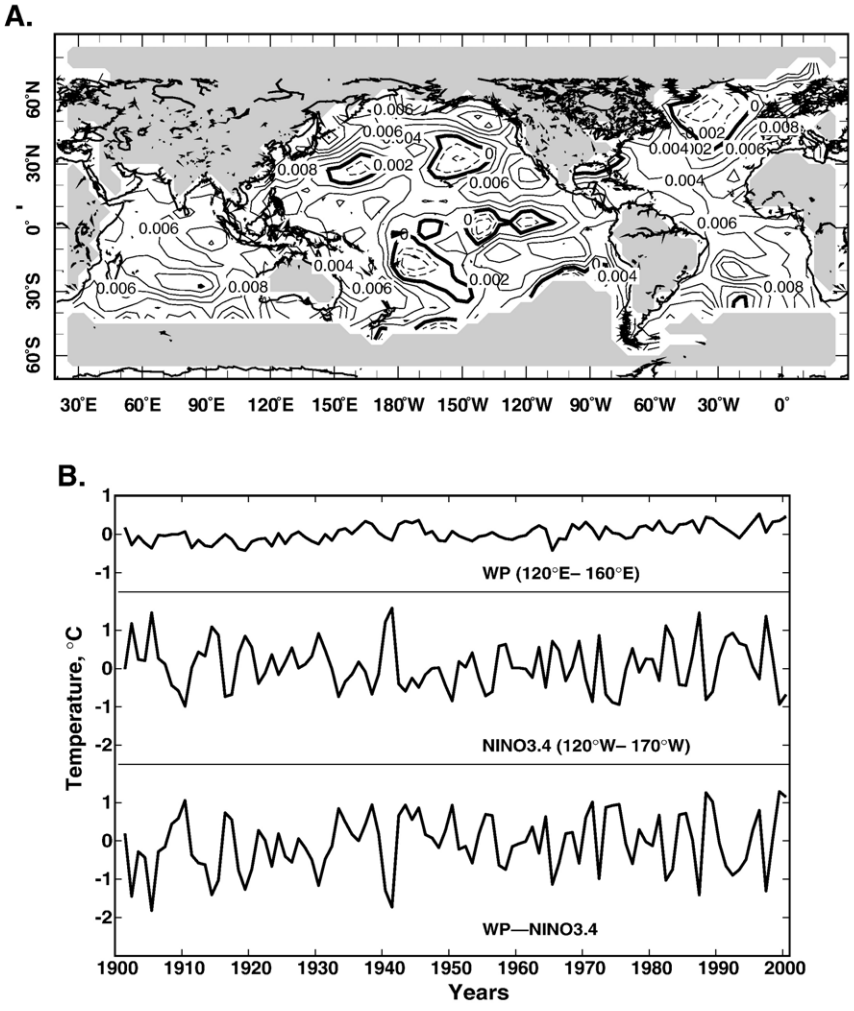

Fig. 20. (A) The trend in monthly mean SST anomalies from 1900 to 2000 in °C per century. Updated from Cane et al. (1997). Regions that cool, such as the eastern equatorial Pacific, are significantly different from the mean global SST warming of 0.4 °C per century. (B) Time series of: (top) the average SST anomaly in the WP region (120° E to 160° E; 5° N to 5° S); (middle) average SST anomaly in the NINO3.4 region (120° W to 170° W; 5° N to 5° S); (bottom) the difference WP-NINO3.4, a measure of the zonal SST gradient. The least squares estimate of the linear trends in the 3 time series (°C per century) are 0.41±0.06, −0.08±0.25, and 0.50±0.25, respectively.

in the central/east Pacific." Some of these model ENSOs had most of their power at a higher frequency (~2 yr) than observed, and most did not have the correct phase with respect to the annual cycle.

Collins and the CMIP Modelling Groups (2005) examined the predictions from 20 CMIP CGCMs forced by a 1% per year increase in greenhouse gases to see whether the mean state becomes more El Niño-like or more La Niña-like. The most probable outcome is no large trend in either direction. Doherty and Hulme (2002) looked at the simulations from 12 CGCMs of changes in the SOI and tropical precipitation from 1900 to 2099. They found that changes in SOI variability are not coherent among the models, broadly consistent with Collins et al. (2005). They do find a slight overall tendency toward a more positive SOI; that is, a more La Niña-like state. Specifically, 6 of the simulations showed a statistically significant positive trend and 2 a statistically significant negative (El Niño-like) trend, while the remaining 4 showed no significant trends.

The positive trend is in keeping with expectations based on the Bjerknes feedback, but was surprising because two of the earliest studies of ENSO in the greenhouse with this generation of models reported a positive (more El Niño-like) trend in NINO3 (Timmermann et al., 1999; Cai and Whetton, 2000). Moreover, the models used in these studies, ECHAM4 and CSIRO, are among those found to have positive trends in the SOI. One possible reason for the discrepancy between the two measures of ENSO is that a trend toward more La Niña-like SSTs in the eastern Pacific is overridden by the overall global warming; as with Fig. 20, it would be revealed by looking at east–west temperature gradients instead of solely at eastern SSTs. Or, it might be that the overall pattern of the ENSO events is altered in the greenhouse world; for example, a shift to the southeast as observed in the late 20th century by Kumar et al. (1999). Doherty and Hulme (2002) found pattern changes in a minority of the 12 simulations they considered, with HADCM2 and ECHAM4 showing eastward shifts.

Recently Liu et al. (2005) have questioned the wisdom of searching for El Niño-like or La Niña-like responses to greenhouse forcing. Instead they examine a number of CGCMs subject to rising greenhouse gases and demonstrate that, instead of a change in the east–west temperature gradient, the common response is for the equatorial Pacific Ocean to warm by more than the subtropical Pacific Ocean. They relate this to changes in the Hadley Cell and surface heat fluxes. From the perspective of the zonal mean atmospheric circulation and mid-latitude drought this `enhanced equatorial warming' is likely to have impacts akin to those of El Niño. As the equator warms so will the tropical troposphere, the jets will move equatorward and strengthen and the transient eddies will drive mid-latitude ascent, increasing precipitation. Anomalous descent, and drying, would instead occur in the subtropics.

Probably the tropical ocean temperatures will respond to greenhouse forcing with some mix of a change in east–west gradient and north–south gradient and there will be attendant changes in stationary waves and the zonal mean atmospheric circulation. The hydrological future of the West will depend on what this mix is. While current models may agree on the north–south gradients they disagree on the east–west gradient and, overall, are too inconsistent to provide much guidance. Perhaps the new generation of coupled GCMs created for the fourth IPCC assessment will show more of a consensus.

Tropical SSTs are not the only influence on how precipitation will change in the greenhouse future. Globally averaged precipitation is expected to increase to balance the increase in surface evaporation, which itself is needed to balance enhanced downward longwave radiation from the atmosphere to the surface. However, the distribution of this increase in precipitation will depend on changes in surface evaporation and changes in atmospheric moisture transport to which ENSO-like changes are only one contributor. Further, a warmer atmosphere can hold more water vapor. Because the water vapor content is influenced by the exponential increase of saturation water vapor content with temperature, while the global increase in precipitation is more linear in temperature, the intensity of precipitation events is expected to increase (Trenberth et al., 2003). This has hydrological implications in that, potentially, more precipitation will go into runoff and less into recharge of soil moisture. Winter snowpack is also expected to decrease in the West reducing the spring melt and gradual recharge of streams and soil moisture at lower levels. See Stewart et al. (2004) and Mote et al. (2005) on this topic as well. These changes that can occur in the absence of circulation changes could also increase the drought risk in North America. Further, if tropical Atlantic SST anomalies really do impact precipitation over North America, the weakening of the Atlantic THC that many model project for the next century would cause cooling in the subtropical North Atlantic which, on the basis of the experiments of Sutton and Hodson (2005), would tend to increase precipitation over parts of North America. Given these complexities it is currently impossible to project what the hydrological future of the Plains and the West will be.

10. Conclusions

Recent advances in the reconstruction of past drought over North America and in modeling the causes of droughts there have provided important new insights into one of the most costly recurring natural disasters to strike North America. A grid of summer PDSI reconstructions has been developed now for most of North America from a remarkable network of long, drought-sensitive tree-ring chronologies. These reconstructions, many of which cover the past 1000 yr, have revealed the occurrence of a number of unprecedented megadroughts over the past millennium that clearly exceed any found in the instrumental records since about AD 1850, including an epoch of significantly elevated aridity that persisted for almost 400 yr over the AD 900–1300 period. In terms of duration, these past megadroughts dwarf the famous droughts of the 20th century, such as the Dust Bowl drought of the 1930s, the southern Great Plains drought of the 1950s, and the current one in the West that began in 1999 and still lingers on as of this writing in 2005.

The impact of the earlier megadroughts on Puebloan and Mississippian agricultural societies, ones based on the clever use of available water resources, is also indicated by the decline and disappearance of those cultures during prolonged drought periods. In turn, the perception of the American West as a place of settlement in the 19th century was strongly influenced by the timing of droughts and wet periods during periods of exploration there.

The extraordinary duration of past North American megadroughts is difficult to explain, but climate models strongly point to tropical Pacific Ocean SSTs as a prime player in determining how much precipitation falls over large parts of North America. Numerical experiments that successfully simulate major droughts over North America from the Civil War to the severe 1999–2004 drought in the West indicate the dominating importance of these SSTs in determining how much precipitation falls over large parts of North America. Of central importance to drought formation is the development of cool "La Niña-like" SSTs in the eastern tropical Pacific region. This development appears to be partially linked to changes in radiative forcing over that region, which affects the Bjerknes feedback mechanism of the ENSO cycle there. Paradoxically, warmer conditions over the tropical Pacific region lead to the development of cool La Niña-like SSTs there, which is drought inducing over North America. La Niña-like conditions were apparently the norm during much of the Medieval period when the West was in a protracted period of elevated aridity and solar irradiance was unusually high. Whether or not this process will lead to a greater prevalence of drought in the future as the world warms due to accumulating greenhouse gases is unclear at this time.

It may well be that the West will luck out as rising greenhouse gases induce an equatorial warming, or an El Niño-like response, and the resulting circulation changes increase precipitation across the mid-latitudes. But we have the nagging reality that a previous time of high positive radiative forcing – the Medieval period – was associated with both colder tropical Pacific SSTs and epic drought across the West. Where the climate system to revert to that severity of drought, conflict, at least on a political level, would return to the West as cities, with relatively modest claims on available water but huge and growing populations, and water-hungry agribusiness, with great political clout, do battle over diminishing resources. The ancient Pueblo migrations may be an unfair analogy, but modern Western society, highly dependent on hydraulic engineering, is yet to be tested by the dreadful droughts we know can occur.

Acknowledgements

The drought reconstructions and their presentation in the North American Drought Atlas were supported by NOAA grant no. NA06GP0450 and NSF grant no. ATM 03-22403, respectively (to ERC). We also gratefully acknowledge the NOAA International Tree-Ring Data Bank and its many contributors for much of the tree-ring data used in this work. In addition, many tree-ring records not yet in the public domain were kindly contributed to the drought reconstruction project by a number of tree-ring scientists doing work in the United States, Canada, and Mexico. All are gratefully appreciated. Contributions of DWS were supported by the NSF Earth System History Program, grant no. ATM 04-00713. RS and MAC were funded in part under the Cooperative Institute for Climate Applications Research (CICAR) award number NA03OAR4320179 from the National Oceanic and Atmospheric Administration, U. S. Department of Commerce. The statements, findings, conclusions, and recommendations are those of the author(s) and do not necessarily reflect the views of the National Oceanic and Atmospheric Administration or the Department of Commerce. RS and MAC also received additional funding from the National Science Foundation (ATM 03-47009). This is Lamont-Doherty Earth Observatory contribution no. 6858.

References

AchutaRao, K., Sperber, K.R., 2002. Simulation of the El Niño Southern Oscillation: results from the Coupled Model Intercomparision Project. Climate Dynamics 19, 191–209.

Acuna-Soto, R., Stahle, D.W., Cleaveland, M.K., Therrell, M.D., 2002. Megadrought and megadeath in 16th century Mexico. Emerging Infectious Diseases 8 (4), 360–362.

Agricultural and Agri-Food Canada, 2002. Drought Watch (for agricultural year 2002). http://www.agr.gc.ca/pfra/drought/maps/archives/e1020830.pdf.2002.

Alley, W.M., 1984. The Palmer Drought Severity Index: limitations and assumptions. Journal of Climate and Applied Meteorology 23, 1100–1109.

Anderson, D.G., Stahle, D.W., Cleaveland, M.K., 1995. Paleoclimate and the potential food reserves of Mississippian societies: a case study from the Savanna River valley. American Antiquity 60, 258–286.

Axtell, R.L., Epstein, J.M., Dean, J.S., Gumerman, G.J., Swedlund, A.C., Harburger, J., Chakravarty, S., Hammond, S., Parker, J., Parker, M., 2002. Population growth and collapse I a multiagent model of the Kayenta Anasazi in Long House Valley. Proceedings of the National Academy of Sciences 99 (suppl. 3), 7275–7279.

Betancourt, J., 2003. The current drought (1999–2003) in historical perspective. Paper Presented at the Southwest Drought Summit, Northern Arizona University, Flagstaff, May 12–13, 2003. Available at http://www.mpcer.nau.edu/megadrought/Betancourt%2520Abstract.pdf.

Bjerknes, J., 1969. Atmospheric teleconnections from the equatorial Pacific. Monthly Weather Review 97, 163–172.

Box, G.E.P., Jenkins, G.M., 1976. Time Series Analysis: Forecasting and Control. Holden Day, San Francisco. 553 pp.

Briffa, K.R., Jones, P.D., Wigley, T.M.L., Pilcher, J.R., Baillie, M.G.L., 1986. Climate reconstruction from tree rings: Part 2, spatial reconstruction of summer mean sea-level pressure patterns over Great Britain. Journal of Climatology 6, 1–15.

Cai, W., Whetton, P.H., 2000. Evidence for a time-varying pattern of greenhouse warming in the Pacific Ocean. Geophysical Research Letters 27, 2577–2580.

Cane, M.A., Clement, A.C., Kaplan, A., Kushnir, Y., Murtugudde, R., Pozdnyakov, D., Seager, R., Zebiak, S.E., 1997. 20th century sea surface temperature trends. Science 275, 957–960.

Clement, A., Seager, R., Cane, M.A., Zebiak, S.E., 1996. An ocean dynamical thermostat. Journal of Climate 9, 2190–2196.

Cobb, C.R., Butler, B.M., 2002. The vacant quarter revisited: late Mississippian abandonment of the Lower Ohio Valley. American Antiquity 67, 625–641.

Cobb, K.M., Charles, C.D., Edwards, R.L., Cheng, H., Kastner, M., 2003. El Niño–Southern Oscillation and tropical Pacific climate during the last millennium. Nature 424, 271–276.

Cole, J.E., Cook, E.R., 1998. The changing relationship between ENSO variability and moisture balance in the continental United States. Geophysical Research Letters 25 (24), 4529–4532.

Cole, J.E., Overpeck, J.T., Cook, E.R., 2002. Multiyear La Niña events and persistent drought in the contiguous United States. Geophysical Research Letters 29 (13). doi:10.1029/2001GL013561.

Collins, M., the CMIP Modelling Groups, 2005. El Niño or La Niña-like climate change? Climate Dynamics 24, 89–104.

Cook, E.R., Stahle, D.W., Cleaveland, M.K., 1992. Dendroclimatic evidence from eastern North America. In: Bradley, R.S., Jones, P.D. (Eds.), Climate Since 1500. Routledge, London, pp. 331–348.

Cook, E.R., Briffa, K.R., Jones, P.D., 1994. Spatial regression methods in dendroclimatology: a review and comparison of two techniques. International Journal of Climatology 14, 379–402.

Cook, E.R., Meko, D.M., Stahle, D.W., Cleaveland, M.K., 1996. Tree-ring reconstructions of past drought across the coterminous United States: tests of a regression method and calibration/verification results. In: Dean, J.S., Meko, D.M., Swetnam, T.W. (Eds.), Tree Rings, Environment, and Humanity. Radiocarbon, Tucson, pp. 155–169.

Cook, E.R., Meko, D.M., Stahle, D.W., Cleaveland, M.K., 1999. Drought reconstructions for the continental United States. Journal of Climate 12, 1145–1162.

Cook, E.R., D'Arrigo, R.D., Cole, J.E., Stahle, D.W., Villalba, R., 2000. Tree-ring records of past ENSO variability and forcing. In: Diaz, H.F., Markgraf, V. (Eds.), El Niño and the Southern Oscillation: Multiscale Variability and its Impacts on Natural Ecosystems and Society. Cambridge University Press, Cambridgep, pp. 297–323.

Cook, E.R., Woodhouse, C.A., Eakin, C.M., Meko, D.M., Stahle, D.W., 2004. Long-term aridity changes in the western United States. Science 306, 1015–1018.

Crowley, T.J., 2000. Causes of climate change over the past 1000 years. Science 289, 270–277.

Dai, A., Trenberth, K.E., Karl, T.R., 1998. Global variations in droughts and west spells: 1900–1995. Geophysical Research Letters 25 (17), 3367–3370.

Dai, A., Trenberth, K.E., Qian, T., 2004. A global dataset of Palmer Drought Severity Index for 1870–2002: relationship with soil moisture and effects of surface warming. Journal of Hydrometeorology 5, 1117–1130.

Deser, C., Phillips, A.S., Hurrell, J.W., 2004. Pacific interdecadal climate variability, linkages between the tropics and north Pacific during boreal winter since 1900. Journal of Climate 17 (16), 3109–3124.

Doherty, R., Hulme, M., 2002. The relationship between the SOI and the extended tropical precipitation in simulations of future climate change. Geophysical Research Letters 29 (10), 1475. doi:10.1029/2001GLO14601.

Douglass, A.E., 1929. The secret of the Southwest solved with talkative tree rings. National Geographic 736–770. December.

Douglass, A.E., 1935. Dating Pueblo Bonito and other ruins of the Southwest. National Geographic Society Contributed Technical Papers. Pueblo Bonito Series, 1, pp. 1–74.

Efron, B., Tibshirani, R., 1986. Bootstrap methods for standard errors, confidence intervals, and other measures of statistical accuracy. Statistical Science 1, 54–77.

Ellison, L., Woolfolk, E.J., 1937. Effects of drought on vegetation near Miles City, Montana. Ecology 18 (3), 329–336.

Evans, M.N., Kaplan, A., Cane, M.A., 2002. Pacific sea surface temperature field reconstruction from coral $\delta^{18}O$ data using reduced space objective analysis. Paleoceanography 17 (1). doi:10.1029/2000PA000590.

Fritts, H.C., 1991. Reconstructing Large-Scale Climatic Patterns from Tree-Ring Data. University of Arizona Press, Tucson, AZ. 286 pp.

Fritts, H.C., Shatz, D.J., 1975. Selecting and characterizing tree-ring chronologies for dendroclimatic analysis. Tree-Ring Bulletin 35, 31–40.

Fritts, H.C., Blasing, T.J., Hayden, B.P., Kutzbach, J.E., 1971. Multivariate techniques for specifying tree-growth and climate relationships and for reconstructing anomalies in paleoclimate. Journal of Applied Meteorology 10, 845–864.

Fye, F., Stahle, D.W., Cook, E.R., 2003. Paleoclimatic analogs to 20th century moisture regimes across the USA. Bulletin of the American Meteorological Society 84 (7), 901–909.

Fye, F., Stahle, D.W., Cook, E.R., 2004. Twentieth-century sea surface temperature patterns in the Pacific during decadal moisture regimes over the United States. Earth Interactions 8, 22 Paper.

Garreaud, R.D., Battisti, D.S., 1999. Interannual and interdecadal variability of the tropospheric circulation in the Southern Hemisphere. Journal of Climate 12, 2113–2123.

Gershunov, A., Barnett, T.P., 1998. Interdecadal modulation of ENSO teleconnections. Bulletin of the American Meteorological Society 79, 2715–2725.

Gu, D., Philander, S.G.H., 1997. Interdecadal climate fluctuations that depend on exchanges between the tropics and extratropics. Science 275, 805–807.

Gumerman, G.J., Dean, J., 2000. Artificial Anasazi. Discovering Archaeology 2, 44–51.

Guttman, N.B., 1998. Comparing the Palmer Drought Index and the Standardized Precipitation Index. Journal of the American Water Resources Association 34, 113–121.

Guttman, N.B., Wallis, J.R., Hosking, J.R.M., 1992. Spatial comparability of the Palmer Drought Severity Index. Water Resources Bulletin 28, 1111–1119.

Hazeleger, W., Visbeck, M., Cane, M.A., Karspeck, A.R., Naik, N.H., 2001. Decadal upper ocean temperature variability in the tropical Pacific. Journal of Geophysical Research 106, 8971–8988.

Heddinghaus, T.R., Sabol, P., 1991. A review of the Palmer Drought Severity Index and where do we go from here? Preprints, Seventh Conference on Applied Climatology, Dallas, TX. American Meteorological Society 242–246.

Heim Jr., R.R., 2002. A review of Twentieth-Century drought indices used in the United States. Bulletin of the American Meteorological Society 83, 1149–1165.

Herweijer, C., Seager, R., 2006. The global footprint of persistent extra-tropical drought In the instrumental era. International Journal of Climatology (in review).

Herweijer, C., Seager, R., Cook, E.R., 2006. North American droughts of the mid to late nineteenth century: a history, simulation and implication for Medieval drought. The Holocene 16, 159–171.

Hoerling, M., Kumar, A., 2003. The perfect ocean for drought. Science 299, 691–694.

Hoskins, B.J., Karoly, K., 1981. The steady response of a spherical atmosphere to thermal and orographic forcing. Journal of the Atmospheric Sciences 38, 1179–1196.

Huang, H.-P., Seager, R., Kushnir, Y., 2005. The 1976/77 transition in precipitation over the Americas and the influence of tropical sea surface temperature. Climate Dynamics 24, 721–740.

Jones, T.L., Brown, G.M., Raab, L.M., McVickar, J.L., Spaulding, W.G., Kennet, D.J., York, A., Walker, P.L., 1999. Environmental imperatives reconsidered: demographic crises in western North America during the medieval climate anomaly. Current Anthropology 40, 137–169.

Jones, P.D., Osborn, T.J., Briffa, K.R., 2001. The evolution of climate over the last millennium. Science 292, 662–667.

Kaplan, A., Cane, M.A., Kushnir, Y., Clement, A.C., Blumenthal, M.B., Rajagopalan, B., 1998. Analyses of global sea surface temperature: 1856–1991. Journal of Geophysical Research 103, 18567–18589.

Kaplan, A., Kushnir, Y., Cane, M.A., 2000. Reduced space optimal interpolation of historical marine sea level pressure: 1854–1992. Journal of Climate 13, 2987–3002.

Karl, T.R., 1983. Some spatial characteristics of drought duration in the United States. Journal of Climate and Applied Meteorology 22, 1356–1366.

Karl, T.R., 1986. The sensitivity of the Palmer Drought Severity Index and Palmer's Z-index to their calibration coefficients including potential evapotranspiration. Journal of Climate and Applied Meteorology 25, 77–86.

Karl, T.R., Koscielny, A.J., 1982. Drought in the United States. Journal of Climatology 2, 313–329.

Karl, T.R., Williams Jr., C.N., Quinlan, F.T., 1990. United States Historical Climatology Network (HCN) serial temperature and precipitation data. Environmental Sciences Division Publication, vol. 3404, p. 371. Available from Carbon Dioxide Information Analysis Center, Oak Ridge National Laboratory, Oak Ridge, TN 37831.

Karspeck, A., Cane, M.A., 2002. Tropical pacific 1976–77 climate shift in a linear, wind driven model. Journal of Physical Oceanography 32, 2350–2360.

Karspeck, A., Seager, R., Cane, M.A., 2004. Predictability of tropical Pacific decadal variability in an intermediate model. Journal of Climate 17, 2842–2850.

Keyantash, J., Dracup, J.A., 2002. The quantification of drought: an evaluation of drought indices. Bulletin of the American Meteorological Society 83, 1167–1180.

Koster, R.D., Dirmeyer, P.A., Guo, Z., Bonan, G., Chan, E., Cox, P., Gordon, C.T., Kanae, S., Kowalczyk, E., Lawrence, D., et al., 2004. Regions of strong coupling between soil moisture and precipitation. Science 305, 1138–1140.

Kumar, K., Rajagopalan, B., Cane, M.A., 1999. On the weakening relationship between the Indian Monsoon and ENSO. Science 284, 2156–2159.

Kushnir, Y., 1994. Interdecadal variations in north-Atlantic sea-surface temperature and associated atmospheric conditions. Journal of Climate 7, 141–157.

Lau, N.-C., A. Leetmaa, A., Nath, M.J., 2006. Attribution of atmospheric variations in the 1997–2003 period to SST anomalies in the Pacific and Indian Ocean basins. Journal of Climate 19, 3607–3628.

Lau, N.-C., Leetmaa, A., Nath, M.J., Wang, H.-L., in press. Influences of ENSO-induced Indo-West Pacific SST anomalies on extratropical atmospheric variability during the boreal summer. Journal of Climate.

Lawrimore, J., Stephens, S., 2003. Climate of 2002 Annual Review. NOAA National Climatic Data Center. http://lwf.ncdc.noaa.gov/oa/climate/research/2002/ann/drought-summary.html.

Lawrimore, J., Heim Jr., R.R., Svoboda, M., Swail, V., Englehart, P.J., 2002. Beginning a new era of drought monitoring across North America. Bulletin of the American Meteorological Society 83, 1191–1192. Available at http://www.ncdc.noaa.gov/oa/climate/monitoring/drought/nadm/nadm-map.html.

Lawson, M.P., Stockton, C.W., 1981. Desert myth and climatic reality. Annals, Association of American Geographers 71, 527–535.

Lean, J.L., Wang, Y.-M., Sheeley Jr., N.R., 2002. The effect of increasing solar activity on the Sun's total and open magnetic flux during multiple cycles: implications for solar forcing of climate. Geophysical Research Letters 29 (24), 2224. doi:10.1029/2002GL015880.

Libecap, G.D., Hansen, Z.K., 2002. 'Rain follows the plow' and dry farming doctrine: the climate information problem and homestead failure in the upper Great Plains, 1890–1925. Journal of Economic History 62, 86–120.

Liu, Z., Vavrus, S., He, F., Weng, N., Zhong, Y., 2005. Rethink tropical ocean response to global warming: the enhanced equatorial warming. Journal of Climate 18, 4684–4700.

Mann, M.E., Cane, M.A., Zebiak, S.E., Clement, A., 2005. Volcanic and solar forcing of El Niño over the past 1000 years. Journal of Climate 18, 447–456.

Mantua, N.J., Hare, S.R., Zhang, Y., Wallace, J.M., Francis, R.C., 1997. A Pacific interdecadal oscillation with impacts on salmon production. Bulletin of the American Meteorological Society 78, 1069–1079.

McGuire, V.L., 2004. Water-level changes in the high plains aquifer, predevelopment to 2003 and 2002 to 2003 (Fact Sheet 2004–3097). Washington, DC, US Geological Survey. Available at http://pubs.usgs.gov/fs/2004/3097/.

Meko, D.M., Cook, E.R., Stahle, D.W., Stockton, C.W., Hughes, M.K., 1993. Spatial patterns of tree-growth anomalies in the United States and southeastern Canada. Journal of Climate 6, 1773–1786.

Milner, G.R., 1998. The Cahokia Chiefdom. Smithsonian Institution Press, Washington. 216 pp.

Mitchell, T.D., Jones, P.D., 2005. An improved method of constructing a database of monthly climate observations and associated high-resolution grids. International Journal of Climatology 25, 693–712.

Mitchell Jr., J.M., Stockton, C.W., Meko, D.M., 1979. Evidence of a 22-year rhythm of drought in the western United States related to the Hale solar cycle since the 17th century. Solar-Terrestrial Influences on Weather and Climate. In: McCormac, B.M., Seliga, T.A. (Eds.), D. Reidel, pp. 125–144.

Mitchell, T.D., Carter, T.R., Jones, P.D., Hulme, M., New, M., 2004. A comprehensive set of high-resolution grids of monthly climate for Europe and the globe: the observed record (1901–2000) and 16 scenarios (2001–2100). Tyndall Working Paper, 55. Tyndall Centre, UEA, Norwich, UK.

Mote, P.W., Hamlet, A.F., Clark, M.P., Lettenmaier, D.P., 2005. Declining mountain snowpack in western North America. Bulletin of the American Meteorological Society 86, 39–49.

Namias, J., 1983. Some causes of United States drought. Journal of Applied Meteorology 22, 30–39.

NASA, 2004. Looking at Earth, "Drought Signals Sever Fire Season in the U.S." Available at http://www1.nasa.gov/vision/earth/lookingatearth/Western_Drought.html.

New, M., Hulme, M., Jones, P.D., 2000. Representing twentieth century space–time climate variability. Part 2: development of 1901–96 monthly grids of terrestrial surface climate. Journal of Climate 13, 2217–2238.

Palmer, W.C., 1965. Meteorological drought. Research Paper, vol. 45. U.S. Weather Bureau.

Pauketat, T.R., 2004. Ancient Cahokia and the Mississippians. Cambridge University Press. 218 pp.

Power, S., Casey, T., Folland, C., Colman, A., Mehta, V., 1999. Inter-decadal modulation of the impact of ENSO on Australia. Climate Dynamics 15 (5), 319–324.

Rayner, N.A., Parker, D.E., Horton, E.B., Folland, C.K., Alexander, L.V., Rowell, D.P., Kent, E.C., Kaplan, A., 2003. Global analyses of sea surface temperature, sea ice, and night marine air temperature since the late nineteenth century. Journal of Geophysical Research 108. doi:10.1029/2002JD002670.

Reisner, M., 1986. Cadillac Desert: the American West and its Disappearing Water. Penguin Books, New York. 582 pp.

Richman, M.B., 1986. Rotation of principal components. International Journal of Climatology 6, 293–335.

Robinson, W.A., 2005. Eddy-mediated interactions between low latitudes and the extratropics. In: Schneider, T., Sobel, A.S. (Eds.), The Global Circulation. Princeton University Press, Princeton, NJ.

Ropelewski, C., Halpert, M., 1987. Global and regional scale precipitation patterns associated with the El Niño/Southern Oscillation. Monthly Weather Review 115, 1606–1626.

Ross, T., Lott, N., 2003. A climatology of 1980–2003 extreme weather and climate events. National Climatic Data Center Technical Report No. 2003-01. NOAA/NESDIS. National Climatic Data Center, Asheville, NC. Available at http://www.ncdc.noaa.gov/ol/reports/billionz.html.

Sahr, R.C., 2005. Inflation conversion factors for dollars 1665 to estimated 2015. Political Science Department, Oregon State University, Corvallis, OR. Available at http://oregonstate.edu/dept/pol_sci/fac/sahr/sahr.htm.

Sauer, C.O., 1980. Seventeenth Century North America. Turtle Island, Berkeley, CA. 295 pp.

Schneider, N., Venzke, S., Miller, A.J., Pierce, D.W., Barnett, T.O., Deser, C., Latif, M., 1999. Pacific thermocline bridge revisited. Geophysical Research Letters 26, 1329–1332.

Schubert, S.D., Suarez, M.J., Region, P.J., Koster, R.D., Bacmeister, J.T., 2004a. On the cause of the 1930s Dust Bowl. Science 303, 1855–1859.

Schubert, S.D., Suarez, M.J., Region, P.J., Koster, R.D., Bacmeister, J.T., 2004b. Causes of long-term drought in the United States Great Plains. Journal of Climate 17, 485–503.

Seager, R., submitted for publication. The turn-of-the-century drought over North America: global context, dynamics and past analogues. Journal of Climate.

Seager, R., Harnik, N., Kushnir, Y., Robinson, W.A., Miller, J., 2003. Mechanisms of hemispherically symmetric precipitation variability. Journal of Climate 16, 2960–2978.

Seager, R., Karspeck, A., Cane, M.A., Kushnir, Y., Giannini, A., Kaplan, A., Kerman, B., Velez, J., 2004. Predicting Pacific decadal variability. In: Wang, C., Xie, S.-P., Carton, J.A. (Eds.), In the Ocean–Atmosphere Interaction. American Geophysical Union, Washington DC, pp. 115–130.

Seager, R., Harnik, N., Robinson, W.A., Kushnir, Y., Ting, M., Huang, H.-P., Velez, J., 2005a. Mechanisms of ENSO-forcing of hemispherically symmetric precipitation variability. Quarterly Journal of the Royal Meteorological Society 131, 1501–1527.

Seager, R., Kushnir, Y., Herweijer, C., Naik, N., Miller, J., 2005b. Modeling of tropical forcing of persistent droughts and pluvials over western North America: 1856–2000. Journal of Climate 18, 4065–4088.

Shabbar, A., Skinner, W., 2004. Summer drought patterns in Canada and the relationship to global sea surface temperatures. Journal of Climate 17 (14), 2866–2880.

Skinner, W.R., Heinze, K., Vincent, L.A., Mekis, E., 2001. The Palmer Drought Severity Index as calculated from the rehabilitated Canadian historical climate database over the 20th Century. Climate Changes: Proceedings of the 2001 Annual Meeting of the Canadian Association of Geographers, Montreal, May 30–June 3, 2001.

Stahle, D.W., Dean, J.S., in press. Tree ring evidence for North American climatic extremes and social disasters. In: Hughes, M.K., Swetnam, T.W., Diaz, H.F. (Eds.), Dendroclimatology: Progress and Prospects. Springer Series "Developments in Paleoecological Research".

Stahle, D.W., Cook, E.R., Cleaveland, M.K., Therrell, M.D., Meko, D.M., Grissino-Mayer, H.D., Watson, E., Luckman, B.H., 2000. Tree-ring data document 16th century megadrought over North America. Eos 81 (12), 121.

Stahle, D.W., Fye, F.K., Therrell, M.D., 2004. Interannual to decadal climate and streamflow variability estimated from tree rings. In: Gillespie, A.R., Porter, S.C., Atwater, B.F. (Eds.), In the Quaternary Period in the United States. Elsevier, Amsterdam, pp. 491–504.

Stegner, W., 1992. Beyond the Hundredth Meridian. Penguin Books, New York. 438 pp.

Stewart, I.T., Cayan, D.R., Dettinger, M.D., 2004. Changes in snowmelt runoff timing in western North America under a 'business as usual' climate change scenario. Climatic Change 62, 217–232.

Stockton, C.W., Meko, D.M., 1975. A long-term history of drought occurrence in western United States as inferred from tree rings. Weatherwise 28, 244–249.

Sutton, R.T., Hodson, D.L.R., 2005. Atlantic Ocean forcing of North American and European summer climate. Science 309, 115–118.

Svoboda, M., LeComte, D., Hayes, M., Heim, R., Gleason, K., Angel, J., Rippey, B., Tinker, R., Palecki, M., Stooksbury, D., Miskus, D., Stephens, S., 2002. The drought monitor. Bulletin of the American Meteorological Society 83 (8), 1181–1190. Available at http://www.drought.unl.edu/dm/monitor.html.

Thomas, D.H., 2000. Exploring Native North America. Oxford University Press. 227 pp.

Timmermann, A., Oberhuber, J., Bacher, A., Esch, M., Latif, M., Roeckner, E., 1999. Increased El Niño frequency in a climate model forced by future greenhouse gas warming. Nature 398, 694–696.

Trenberth, K.E., Branstator, G.W., Karoly, D., Kumar, A., Lau, N.-C., Ropelewski, C., 1998. Progress during TOGA in understanding and modeling global teleconnections associated with tropical sea surface temperature. Journal of Geophysical Research 103, 14291–14324.

Trenberth, K.E., Dai, A., Rasmusson, E.M., Parsons, D.B., 2003. The changing character of precipitation. Bulletin of the American Meteorological Society 37, 129–148.

USDA, 2004. Natural resources conservation service. National Water and Climate Center. Reservoir Storage as of May 1, 2004. Available at http://www.wcc.nrcs.usda.gov/cgibin/resvgrph2.pl?area%=west&year=2004&month=05.

van der Schrier, G., Briffa, K.R., Jones, P.D., Osborn, T.J., 2006a. Summer moisture availability across Europe. Journal of Climate 19, 2818–2834.

van der Schrier, G., Briffa, K.R., Osborn, T.J., Cook, E.R., 2006b. Summer moisture availability across North America. Journal of Geophysical Research 111, D11102. doi:10.1029/2005JD006745.

Warrick, R.A., 1980. Drought in the Great Plains: a case study of Research on Climate and Society in the USA. In: Ausubel, J., Biswas, A.K. (Eds.), Climatic Constraints and Human Activities, pp. 93–123. IIASA Proceedings Series, vol. 10. Pergamon Press, New York.

Weaver, J.E., Albertson, F.W., 1936. Effects of the Great Drought on the prairies of Iowa, Nebraska, and Kansas. Ecology 17, 567–639.

Wells, N., Goddard, S., Hayes, M.J., 2004. A self-calibrating Palmer Drought Severity Index. Journal of Climate 17, 2335–2351.

Wheeler, D.L., 1991. The blizzard of 1886 and its effect on the range cattle industry in the southern Plains. Southwestern Historical Quarterly 94.

Wilber, C.D., 1881. The Great Valley and Prairies of Nebraska and the Northwest. Daily Republican Print, Omaha, NB. 382 pp.

Williams, S., 1990. The Vacant Quarter and other late events in the Lower Valley. In: Dye, D.H., Cox, C.A. (Eds.), Towns and Temples Along the Mississippi. University of Alabama Press, Tuscaloosa, pp. 170–180.

Woodhouse, C.A., Overpeck, J.T., 1998. 2000 years of drought variability in the central United States. Bulletin of the American Meteorological Society 79, 2693–2714.

Woodhouse, C.A., Kunkel, K.E, Easterling, D.R., Cook, E.R., 2005. The twentieth-century pluvial in the western United States. Geophysical Research Letters 32, L07701. doi:10.1029/2005GL022413.

Worster, D., 1979. Dust Bowl: the southern plains in the 1930s. Oxford University Press, New York. 227 pp.

Worster, D., 1985. Rivers of Empire: Water, Aridity and the Growth of the American West. Pantheon Books, New York, p. 402.

Zebiak, S.E., Cane, M.A., 1987. A model El Niño–Southern Oscillation. Monthly Weather Review 115, 2262–2278.

Zhang, Y., Wallace, J.M., Battisti, D.S., 1997. ENSO-like decade-to-century scale variability. 1900–93. Journal of Climate 10, 1004–1020.

Zhang, Z., Mann, M.E., Cook, E.R., 2004. Alternative methods of proxy-based climate field reconstruction: application to summer drought over the conterminous United States back to AD 1700 from tree-ring data. The Holocene 14 (4), 502–516.